FDM: the Filter Diagonalization Method for data processing in NMR experiments.

Vladimir A. Mandelshtam

Chemistry Department, University of California, Irvine, CA 92697-2025,

E-mail: mandelsh@uci.edu

CONTENTS.

Important notations. A linear operator is identified by a cap: $\hat{A}$. In the expression $|b) = \hat{A}|c)$ a vector $|c)$ from a linear space is mapped to a vector $|b)$ from the same space. $(c|$ defines a dual vector to $|c)$ and $(c|b) = (b|c)$, complex symmetric (as opposed to the Hermitian $\langle c|b\rangle = \langle b|c\rangle^*$) inner product between the two vectors $|c)$ and $|b)$. Bold characters, as $\mathbf{A}$ or $\mathbf{C}$ are used for matrix representations of linear operators or vectors. Their elements are then defined using the following notations: $[\mathbf{A}]_{mn}$ or $[\mathbf{C}]_n$. $\mathbf{A}^{\mathrm{T}}$ is a transpose of matrix $\mathbf{A}$, while $\mathbf{A}^\dagger$, is its adjoint (transposed and complex conjugated) matrix.

1. INTRODUCTION AND HISTORICAL REMARKS.

The main goal of this article is to review the *Filter Diagonalization Method* (FDM), a method of spectral analysis of time signals and, in particular, the NMR signals. We discuss various aspects of NMR data processing in the framework of FDM. Most results reported here were published previously [1-16]. An attempt is made to present FDM critically, emphasizing both its advantages and drawbacks. Some unsolved either conceptual or computational challenges, associated mostly with the multidimensional FDM, are identified.

We start with a description of some aspects of the spectral analysis of quantum dynamical systems bacause of the obvious historical and conceptual connections between the quantum dynamics calculations and FDM.

Resonances or quasi-bound states appear to be one of the most important characteristics of an open or dissipative quantum system (as, e.g., a scattering system). The calculation of resonance parameters has always been a very important numerical task in the study of quantum dynamics. Unlike the bound states, resonances, formally defined as the complex poles of the Green's function, are better characterized by complex energies with the imaginary parts associated with the inverse lifetimes. This often required replacement of the true Hermitian Hamiltonian by a non-Hermitian one with the imaginary part effectively describing the dissipation. The eigenvalues of such an effective Hamiltonian are complex and could, therefore, approximate the true poles of the Green's function. As such the arising numerical problem would be the one of diagonalizing a non-Hermitian Hamiltonian matrix. Diagonalization of a large non-Hermitian matrix still remains a central numerical bottleneck in quantum dynamics calculations: the conventional methods based on matrix transformations have severe numerical limitations, while iterative techniques with better numerical scaling, such as the Lanczos method, are generally unstable.

"Filter Diagonalization" was the name given by Neuhauser [17] in 1990 to a numerical procedure to compute eigenenergies of a possibly large quantum system using solutions of the time-dependent Schrödinger equation. In conventional, so called, spectral methods based on, say, Fourier transforming a time correlation function,

$$c(t) = \langle 0|e^{-i\frac{t}{\hbar}\hat{H}}|0\rangle \ , \tag{1}$$

the propagation would have to be performed for the time defined by the Heisenberg uncertainty principle, $t \sim \hbar/\delta E$ for a given energy resolution δE. Note that in Eq. 1 we used the Dirac "bra", $\langle 0|$, and "ket", $|0\rangle$, notations for a wavefunction. In the Filter Diagonalization the propagation time required to achieve similar resolution could be much shorter: the "filter" part would then be responsible for constructing a set of "good" basis functions filtered by a short-time Fourier transform (FT),

$$|\varphi_j\rangle = \int_0^{t_{\max}} e^{i\frac{t}{\hbar}(\varphi_j - \hat{H})}|0\rangle dt \ , \tag{2}$$

while the "diagonalization" of the Hamiltonian matrix $H_{jj'} = \langle\varphi_j|\hat{H}|\varphi_{j'}\rangle$, evaluated in this basis, would deliver the accuracy for the eigenenergies beyond the Heisenberg uncertainty relation. Because the Fourier basis is highly localized in the energy space, i.e., each basis function $|\varphi_j\rangle$ is dominated by just a few eigenfunctions of $\hat{H}$ with eigenvalues close to φ_j, the narrow band Fourier basis with φ_j values chosen in a small energy interval can represent the eigen subspace in this interval. Since 1990 this idea, originally implemented quite naively, had undergone certain transformations before it boiled down to numerically competitive schemes. One of the early real successes of the Filter Diagonalization was the very accurate calculation of hundreds of quantum scattering resonances of the HO_2 radical [18], which is still hard to reproduce by any other technique.

The most essential development, that gave a new perspective to the Filter Diagonalization, was published by Wall and Neuhauser [1] in 1995. In this article it was discovered that neither the Fourier basis functions $|\varphi_j\rangle$ (Eq. 2) nor the Hamiltonian operator $\hat{H}$ have to be known explicitly to carry out the Filter Diagonalization steps: once a time correlation function $c(t)$ is available, the Hamiltonian matrix could be evaluated from it.

Since, on the other hand, we can write

$$c(t) = \sum_{k=1}^{K} d_k e^{-it\omega_k} \ , \tag{3}$$

where $\omega_k = E_k/\hbar$ are proportional to the eigenvalues of $\hat{H}$ and the amplitudes $d_k = |\langle 0|\omega_k\rangle|^2$ are defined by the projections of the eigenfunctions $|\omega_k\rangle$ on the initial state $|0\rangle$, the Filter Diagonalization could be applied to extract the frequencies ω_k and the amplitudes d_k from a general time signal $c(t)$ only assuming that Eq. 1 is satisfied, even in the case, when the time signal $c(t)$ was not generated by a quantum Hamiltonian. In this case $\hat{H}$ plays a role of an effective Hamiltonian whose spectral parameters are extracted by the filter diagonalization procedure. As such the method was applied to extract the instantaneous normal modes from a time signal generated by calculating the classical trajectories of a multi-particle system [19]. However, the numerical implementation of the finding of ref. [1] was quite inefficient, so it would remain just a curious observation, unless better implementations [2, 20] could be found later. For example, in ref. [2], the new version of the method was shown to possess the properties of an optimal method of solving Eq. 3 from several points of view including convergence, speed and reliability. To distinguish this efficient version and its further extensions from all the previous ones, but to also keep the original name, we call it FDM (the Filter Diagonalization Method). Later FDM was applied to a number of problems in theoretical physics and chemistry (some selected references are [21-31]), where solution of the *Harmonic Inversion Problem* (HIP), as defined by Eq. 3, was essential. At the same time FDM started to be applied to NMR data processing (the early publications include [4-8]. One point, which might not always seem obvious, is that formally Eq. 3 is a non-linear fit problem with all the bad attributes of the non-linearity. In particular, a general non-linear optimization problem does not have a unique solution. Moreover, finding a solution for such a problem might become a serious numerical challenge even with a few fitting parameters. Apparently, the HIP, being only formally nonlinear, is not that in reality, once it is formulated appropriately. One of the central advantages of FDM (shared by several other linear algebraic techniques) is that the spectral parameters are, to certain extent, uniquely obtained by solving some particular linear algebraic problems. Originally, the authors of refs. [1, 2] were not aware of the vast number of the high resolution methods for spectral analysis of time signals, so some aspects of FDM were actually re-inventions. In fact, the first known publication on the subject, that contained several key ideas used in FDM as well as in most other methods of solving Eq. 3, is due to Baron de Prony and dated by 1795 [32]. In particular, the first linear algebraic solution to a problem of identifying the parameters of a multi-exponential decay of a time signal was presented in the same article by Baron de Prony. It might appear that for the period of more than two centuries the problem must have been beaten to death. In spite of that, it is still alive and FDM seems to possess some unique features which, in certain respects, makes it superior to the other methods. In particular, to the best of our knowledge, its multidimensional versions hardly have competing analogues. Although, for some 1D problems, especially involving very long and noiseless signals, FDM is extremely efficient, its actual strength is revealed outside of the 1D applications. The basic reason is that FDM processes the whole multidimensional data set simultaneously by fitting it to a certain multidimensional parametric form, unlike the FT spectral analysis which is intrinsically one-dimensional. For instance, 2D HIP can be written as

$$c(t_1, t_2) = \sum_{k=1}^{K} d_k e^{-it_1\omega_{1k}} e^{-it_2\omega_{2k}} \tag{4}$$

with ω_{1k}, ω_{2k} and d_k now characterizing the 2D spectral features. By solving Eq. 4 one can, in principle, obtain high spectral resolution even if the signal is not available at both long t_1 and t_2, as would be required by the Fourier uncertainty principle. It is the total size of the 2D data set, which implies the total number of algebraic equations with the unknowns $\{d_k, \omega_{1k}, \omega_{2k}\}$ and which is relevant. Experimentally, it may be easy to satisfy the condition when the total number, $N_1 \times N_2$, of the 2D signal points, i.e., the number of equations, dominates the total number of unknowns $(3K)$. In a 1D signal processing scheme the length of the signal in <u>each</u> dimension has to dominate the number of unknowns, i.e. $N_1 > 2K$ and $N_2 > 2K$. In ref. [6] one can find a striking example of a resolved 2D double-absorption HSQC spectrum obtained using just <u>two</u> 1D purely phase modulated FIDs.

Unfortunately, 2D FDM did not always work as well as it was predicted by the naive information consideration. In fact, the original formulation of 2D FDM [3] has only been applied to either model or experimental NMR signals [6, 5] with quite high signal to noise ratio (SNR) for which the assumption of Eq. 4 holds. The attempts to treat more complex and noisier multi-dimensional data by the method of ref. [3] identified some problems, that were addressed in several recent papers [8, 9, 10, 12]. For example, in ref. [8] it was pointed out that a problem would occur if there are degenerate frequencies, i.e., when the 2D spectra would have peaks at the same ω_{1k} but separated in the other frequency dimension (or *vice versa*). A method implemented in the frame of 2D FDM, called "simultaneous diagonalization", was suggested to overcome this degeneracy problem. It was argued later [10] that the degeneracy itself does not actually create any numerical problem, if the SNR is sufficiently high, an artifact free spectrum can be constructed by using the *resolvent operator* (or the *Green's function*) approach [9, 10, 12]. Rather than Eq. 4, this approach implies a much more pessimistic, direct-product, parametric form to represent the 2D time domain data

$$c(t_1,t_2) = \sum_{k_1=1}^{K_1} \sum_{k_2=1}^{K_2} d_{k_1 k_2} e^{-it_1\omega_{1k_1}} e^{-it_2\omega_{2k_2}} \ , \tag{5}$$

although this equation is not solved explicitly for the unknowns $d_{k_1 k_2}$, ω_{1k_1} and ω_{2k_2}. Apparently, Eq. 5 coincides with the form used previously for parametric classification of 2D NMR signals [33, 34, 35, 36].

Although the resolvent operator approach appeared to be a significant improvement, compared to the previous implementations of 2D FDM, i.e., it significantly lowered the SNR threshold of the FDM stability, it would still fail for sufficiently noisy data, where the FT spectra could still be very well resolved. The reason is that for a general 2D data array $c(t_1,t_2)$ Eq. 4 is ill-defined or, in other words, the solution is very sensitive to both the parameters of the fit (such as K) and small perturbations of $c(t_1,t_2)$. This sensitivity causes instability of the result for a noisy input, appearing in the FDM spectra in a wild non-linear fashion as spurious spikes or errors in the amplitudes and phases of the genuine features.

The next development which gave FDM new breath was the discovery of a simple trick to overcome the instability problem. The idea was to average the FDM spectrum over those small perturbations of the input to which the former is so sensitive. The original implementation of the averaging idea [9, 10, 13] used variation of the signal size processed by FDM. However a more consistent and elegant way to average suggested in ref. [12] is based on averaging the FDM spectrum over small random perturbations of the input signal of fixed size. The fact that a particular realization of the signal plus artificial noise has more noise than the original signal is irrelevant as the auxiliary artificial noise has zero mean. We called this latter method *pseudo-noise averaging*.

The Green's function formalism with the averaging were two of the main ingredients in the status of the multidimensional FDM until the very end of the 20-th century. Apparently, irrelevant of the fact that FDM is based on solving the parametric fit equation (4) these two methods complicate a direct parametric classification of the spectrum in terms of frequencies and amplitudes, as each spectral peak is now characterized by many terms with a lot of cancellations and interferences. In a sense, this is a step backwards comparing with the original hopes of refs. [3, 5, 6]. Thus construction of a compact and reliable line list for noisy data in more than one dimension at this stage reappeared as an unsolved problem. The other problem, albeit not conceptual, is that averaging requires multiple diagonalizations which make FDM by one or two orders of magnitude more time consuming. One step toward reduction of both the ill-conditioned structure of the matrices involved and the computational burden was to try to implement a more sophisticated multiscale Fourier basis [11]. In the most simple implementation, a two-scale basis represents two subspaces, a narrow band Fourier basis (i.e., dense in the frequency domain and long in the time domain) which is localized in the particular small frequency window and describes the fine structure in this window, and a coarse basis (i.e., sparse in the frequency domain and short in the time domain) that describes global low resolution behaviour of the spectrum. Such a multiscale basis is not only capable of minimizing the total size of the basis, but for some difficult cases it gives a more stable solution, especially in the case of both low SNR and the presence of broad non-localized spectral features, where the original method fails, even in the 1D case.

The new Millennium has been marked with breakthroughs in both improving the performance of multidimensional FDM and the problem of spectral estimation. It appeared [14] that the spectral estimation problem could be handled more consistently in the framework of the resolvent (or the Green's function) formula, e.g., $I(s) = \mathbf{C}^{\mathrm{T}}\mathbf{R}^{-1}\mathbf{C}$, where $\mathbf{R} = \mathbf{R}(s)$ and $\mathbf{C}$ are data matrices defined by the time signal. $I(s)$ does not, in principle, require calculation of the spectral parameters as it can be evaluated directly by matrix inversion or by solution of a linear system. Since the data matrix $\mathbf{R}$ is singular, a pseudo-inverse $\mathbf{R}_q^{-1}$ must be used. In the new numerical expression for spectral estimation, called the *Regularized Resolvent Transform* (RRT) the Singular Value Decomposition (SVD) or Tikhonov regularization [41] is implemented for regularization purpose. In the latter case the regularized inverse is approximated by $\mathbf{R}_q^{-1} \approx \left(\mathbf{R}^{\dagger}\mathbf{R} + q^2\right)^{-1}\mathbf{R}^{\dagger}$. Possible singularities of $\mathbf{R}^{-1}$ are removed by using the real regularization parameter q. The latter actually controls the appearance of artifacts: a larger value of q suppresses the artifacts and broadens the peaks with low amplitudes. A too large q leaves only a few strongest peaks in the spectrum. The role of q is, therefore, similar in spirit to that of the singular value threshold in the truncated SVD applications but is generally much less frustrating as the result only smoothly depends on q. Unlike FDM, RRT has the status of a "transform", i.e., a direct (albeit non-linear) transformation of the time-domain data into the frequency domain spectrum and is very straightforward to use. Unfortunately, in RRT no line list is produced which may be associated with its major drawback. Another difficulty associated with the RRT at this stage is the lack of a numerically fast method to evaluate the absorption spectrum directly from a single multidimensional purely phase modulated signal. Thus, in spite of the invention of RRT, FDM had not lost its attractiveness as it can, at least in principle, deliver the spectral parameters with the possibility of easily generating all kinds of spectral representations.

FDM2k was the name given to the new version of FDM [15] that used a simple trick to remove the instability in the solution of the arising generalized eigenvalue problems avoiding either expensive averaging over many FDM calculations or the state of the art fiddling with various FDM parameters. In FDM2k a real parameter q, similar to that in RRT, is used to control the appearance of the artifacts. However, so far FDM2k has been tested only for 2D applications, while higher dimensional applications may have some caveats.

Despite the very encouraging results obtained so far, FDM is very far from being able to entirely replace the FT data processing. Clearly, the latter has quite different requirements to the data, such as no restrictions to the lineshapes or lower bounds for SNR, but it needs bigger data sets in all dimensions. FDM can extract certain types of spectral information that are unavailable by FT. For example, in 2D FT data processing purely phase modulated signals give rise to mixed-phase ("phase-twist") lineshapes in which neither the real nor the imaginary part of the 2D FT spectrum can be phased to the desired double absorption lineshape [37]. In some experiments the latter can be obtained by, for instance, acquiring hyper-complex type data [38] corresponding to twofold larger data sets. However, in 2D-J experiments those are unavailable and only absolute value 2D spectra [39] are used, leading to poor resolution even when the data sets are large or requiring implementation of heavy digital filters [40] to improve the lineshapes at the expense of considerable amplitude distortions. In FDM one can generate a double-absorption spectrum from purely phase modulated data, or an absorption mode 45^o projection of a 2D-J spectrum leading to a singlet-proton spectrum. The latter idea is extendable to more than 2D experiments, such as 3D HSQC-J and 4D J-TOCSY-J [13], in which the proton multiplets are collapsed into singlets, considerably simplifying the problem of spectral assignment. Thus, FDM not only allows one to improve the spectral resolution relative to the conventional data processing, but also makes certain experiments much more useful, and opens various possibilities to design new experiments.

2. SPECTRAL ESTIMATORS, PARAMETER ESTIMATORS AND NON-LINEAR PROBLEMS.

For a given 1D time signal $c_n \equiv c(t_n)$ defined on a finite time grid $t_n,\ n = 0, ..., N-1$ we can formulate the spectral analysis problem. In this section we will describe the difference and relation between a spectral estimator and parameter estimator. Although in general t_n could be any grid, due to various reasons it is most common to consider equidistant time points, $t_n = n\tau$, separated by a sufficiently small step τ, which is consistent with the spectral width according to

$$\tau = \frac{2\pi}{SW} \ , \tag{6}$$

i.e., so that the highest frequency oscillation is correctly represented by the discretized data.

We can now define two spectral functions corresponding to the integral FT,

$$I(s) = i \int_0^\infty c(t) e^{its} dt \ , \tag{7}$$

and discrete FT (DFT),

$$I^\tau(s) = i\tau \sum_{n=0}^{\infty} \left(1 - \frac{\delta_{n0}}{2}\right) c_n e^{in\tau s} \ , \tag{8}$$

where the term $\left(1 - \frac{\delta_{n0}}{2}\right)$ multiplies c_0 by $\frac{1}{2}$ to correct the error introduced by the discrete sum approximation of the continuous half-line Fourier integral. Generally, for small τ we have $I^\tau(s) \approx I(s)$ but unlike $I(s)$, the DFT spectrum $I^\tau(s)$ is periodic in s with the period equal to the Nyquist width $\frac{2\pi}{\tau}$. Since $c(t)$ is not available on the whole semi-infinite interval $[0, \infty)$ and since the experimental data may also be contaminated by noise, it is impossible to use Eq. 7 directly to compute $I(s)$ (or $I^\tau(s)$). A method which estimates $I(s)$ (or $I^\tau(s)$) from the available incomplete and possibly noisy data can be called a *spectral estimator*. It is, therefore, more appropriate to formulate the spectral estimation problem as the following integral equation, obtained from Eq. 7 by the inverse FT,

$$c_n = \frac{i}{2\pi} \int_{-\infty}^{\infty} I(s) e^{-it_n s} ds \ , \ n = 0, ..., N-1 \ . \tag{9}$$

Apparently, a finite DFT is an example of a linear method of solving Eq. 9, i.e., DFT is a spectral estimator, in which the infinite time FT spectrum is estimated by a finite sum. It is not necessary to explain the importance of DFT for the problem of spectral analysis. DFT is computationally very efficient, due to the existence of fast Fourier transform (FFT) algorithms, and robust method. It gives a uniform approximation of the spectrum. In particular, the resolution of the FT spectrum is not worse than

$$\delta s \sim \frac{2\pi}{N\tau} \ , \tag{10}$$

which is due to the relation between the frequency grid spacing and the Fourier length $N\tau$. Furthermore, the FT spectrum is stable with respect to the variations of the signal. This is due to the linear nature of Eq. 8, the time domain noise being converted into the frequency domain noise linearly.

Having mentioned the main advantages of FT spectral analysis, it is also important to point out some of its drawbacks, such as finite resolution, *Gibbs oscillations*, etc. Also, because of the finite time step τ the estimated lineshapes of the broad lines in $I^\tau(s)$ are distorted. However, this particular problem is practically irrelevant and, if necessary, can be avoided by decreasing τ. It is the truncation artifacts which are the major disadvantage of the Fourier spectral estimators. To reduce the Gibbs oscillations it is customary to use *apodization* of the signal prior to the FT, i.e., multiplication of c_n by some smoothly decaying function of n. The "uncertainty relation" between the frequency and time, Eq. 10, responsible for the uniform resolution of the FT, also turns into a major disadvantage as the FT resolution cannot be better than that in Eq. 10.

To this end, let us note that there are other than FT methods of solving Eq. 9, the Maximum Entropy Method (MEM) being the most popular in NMR (see, e.g., [42, 43]). It is straightforward to formulate the inversion problem, Eq. 9, as a non-linear least squares problem. The main characteristics of the nonlinear optimization methods is, theoretically, their high resolution nature, which is different from Eq. 10. On the other hand, a major caveat associated with nonlinear problems is the existence of many local minima solutions, i.e., difficulties in finding the global minimum, and their notoriously ill-defined nature. Even though a non-linear method can, in principle, offer very high resolution, our goal here is to avoid dealing with such problems, as we consider them too difficult to apply and, generally, very time consuming.

A *parameter classification* in NMR data processing is commonly understood as the following parametric fit of the time signal (FID),

$$c_n = \sum_{k=1}^{K} d_k e^{-in\tau\omega_k} , \tag{11}$$

where again we restrict the consideration to the case of a finite equidistant time grid with $n = 0, ..., N-1$. In Eq. 11 the variational parameters are the complex amplitudes d_k and complex frequencies $\omega_k = \nu_k - i\gamma_k$. The line width γ_k is proportional to the inverse decay time for the term that oscillates with (real) frequency ν_k.

This problem is often referred to as the *Harmonic Inversion Problem* (HIP). At first glance, it might appear that there is nothing special in the form of Eq. 11. However, the HIP is the most popular among all the other possible parametric forms. The reason is its unique property of having a linear algebraic solution and, therefore, allowing one to consider a much bigger parameter space than that usually considered feasible in non-linear optimization problems.

There is a hidden subtlety in the formulation of HIP which will arise if one tries to assume the total number of terms K to be fixed and N independent. This seemingly natural assumption fails as it makes the problem very ill-defined and the solution very sensitive to the errors (noise) in the input data. Even starting with a very special case, i.e., $K < N/2$, a general infinitesimal perturbation of the input signal c_n will destroy this special property. Therefore, the well-defined, i.e., numerically stable, formulation of HIP is to set $K = N/2$ (considering, without serious sacrifice, only even N) which corresponds to having the number of unknowns consistent with the number of equations. In the context of FDM the total number of terms in Eq. 11 is usually irrelevant because the spectral analysis is generally performed locally in the frequency domain. In this case it is more appropriate to think in terms of the density of information in the frequency domain, i.e., the local density of poles $\rho(\omega_k)$ that should be consistent with the information content of the signal c_n of size N,

$$\rho(\omega_k) \equiv \frac{1}{\Delta\omega_{\rm aver}} \sim \frac{N\tau}{4\pi} , \tag{12}$$

where $\Delta\omega_{\rm aver}$ is the local average spacing between the poles. This condition is to be compared with the FT uncertainty principle, Eq. 10. Clearly, Eq. 12 offers much higher resolution than the latter for the time signals that are well represented by the form of Eq. 11.

Rigorously speaking, the solution of Eq. 11 is not unique as the line list $\{\omega_k, d_k\}$ depends on the size N of the fitted data set. In which sense then can we consider the line list converged? Depending on the type of the problem, Eq. 11, can be understood differently. One extreme corresponds to having to find the spectral parameters for a very large data set c_n with very dense set of spectral lines and with sufficiently high SNR. This situation appears to be quite typical in NMR and is most favorable for FDM but generally difficult to handle using other high resolution methods involving solutions of large linear algebraic problems. The other extreme considered typically in the engineering literature corresponds to having to extract the parameters of a few genuine lines (sources) from the sea of noise. In the present article we do not consider the latter case, assuming that the form of Eq. 11 is an efficient representation of the data and that the peaks with large amplitudes are not due to noise, but rather the noise is represented by either broad poles ω_k or small amplitudes d_k or both. Therefore, once we achieved the regime when a certain part of the line list is not sensitive to further increase of the data size, while there are still entries (ω_k, d_k) that change with N, we can consider the stable part of the line list converged, although the degree of convergence will always be a very delicate issue.

In addition to the line list it is often desirable to have a spectrum $I(s)$ as a function of the real frequency argument s, as the spectral representation is much less ambiguous than the line list. It is also important to realize that solution of Eq. 11 for the line list is much more demanding than constructing the spectrum by solving Eq. 9, as the latter does not yield the line list, while the line list generally yields the spectrum. In other words, a parameter estimator can often be used as a spectral estimator (but not *vice versa*). The simplest example of a spectral estimation using the line list $\{\omega_k, d_k\}$ is based on analytic integral or discrete FT of Eq. 11 resulting in

$$I(s) = \sum_k d_k G_k(s) \tag{13}$$

or

$$I^\tau(s) = \sum_k d_k G_k^\tau(s) \ , \tag{14}$$

where we introduced the two complex resolvent functions (Lorentzians)

$$G_k(s) = i \int_0^\infty e^{it(s-\omega_k)} = \frac{1}{\omega_k - s} \tag{15}$$

and

$$\begin{aligned} G_k^\tau(s) &= i\tau \sum_{n=0}^\infty \left(1 - \frac{\delta_{n0}}{2}\right) e^{in\tau(s-\omega_k)} \\ &= \frac{i\tau}{1 - e^{i\tau(s-\omega_k)}} - \frac{i\tau}{2} \ . \end{aligned} \tag{16}$$

For small values of $\tau(s-\omega_k)$ we have $G_k(s) \approx G_k^\tau(s)$, however, unlike $G_k(s)$, $G_k^\tau(s)$ is periodic with period equal to the Nyquist width $\frac{2\pi}{\tau}$.

In NMR spectroscopy the absorption spectrum is the physically most meaningful. Note, that in the 1D case it is usually possible to express

$$A(s) = \mathrm{Im}\{I(s)\} \ , \tag{17}$$

assuming all amplitudes d_k being real and $I(s)$ properly phased. Since in the framework of the FT spectral analysis no other absorption mode representation is available, Eq. 17 is called the absorption spectrum, even in cases when different amplitudes are not in phase resulting in non-absorption lineshapes. It is, therefore, useful to have a more general definition of an absorption spectrum in which the absorption lineshapes are reinforced but which would coincide with the usual expression if all amplitudes have zero phase:

$$A(s) = \sum_k d_k \delta_k(s) \ , \tag{18}$$

$$A^\tau(s) = \sum_k d_k \delta_k^\tau(s) \tag{19}$$

with

$$\delta_k(s) \equiv \mathrm{Im}\left\{G_k(s)\right\} \equiv \mathrm{Im}\left\{\frac{1}{\omega_k - s}\right\} \ , \tag{20}$$

$$\delta_k^\tau(s) \equiv \mathrm{Im}\left\{G_k^\tau(s)\right\} \equiv \mathrm{Im}\left\{\frac{i\tau}{1-e^{i\tau(s-\omega_k)}}\right\} - \frac{\tau}{2} \ . \tag{21}$$

Apparently, $\delta_k(s)$ is the familiar absorption Lorentzian lineshape, $\frac{\gamma_k}{(\nu_k-s)^2+\gamma_k^2}$, centered at $\nu_k \equiv \mathrm{Re}\left\{\omega_k\right\}$ and having the width $\gamma_k \equiv \mathrm{Im}\left\{\omega_k\right\}$. Furthermore, in the case of zero width both $\delta_k(s)$ and $\delta_k^\tau(s)$ coincide with the Dirac delta-function (multiplied by 2π).

Note that both $A(s)$ and $A^\tau(s)$ will generally be complex if the amplitudes are not phased. A real-valued absorption mode spectrum can then be obtained by using either the real part of an *a priori* phased $A(s)$ or the absolute value of $A(s)$.

In the 1D case we will use the standard and familiar definition of an absorption spectrum (17) if not explicitly specified otherwise.

Being very simple analytic representations of the spectrum, the sum of Lorentzians, Eqs. 13, 14, 18 and 19, are clearly very useful in many respects. Later in the text we will address the question of how well the spectrum can be estimated by these forms using FDM and when the representations fail.

3. NON-HERMITIAN QUANTUM MECHANICS: CONNECTION TO THE HARMONIC INVERSION PROBLEM (HIP).

In this section we review the quantum mechanical terminology and relations to be used in FDM to solve the HIP. Clearly, the method could be presented without the quantum mechanical jargon, although the latter makes the theory more elegant and all the derivations, straightforward.

The conventional quantum mechanics considers only Hermitian operators acting in a Hilbert space. The latter is characterized by a Hermitian inner product $\langle\Psi|\Phi\rangle = \langle\Phi|\Psi\rangle^*$ with the asterisk defining the complex conjugate. This has many useful consequences. For example, for any vector Ψ from the Hilbert space we can define the norm, $\langle\Psi|\Psi\rangle$, which is always a real number; the eigenvalues of a Hermitian operator are real. One can actually restrict consideration to the use of real numbers exclusively by choosing a real basis. In such a basis a Hermitian operator becomes real symmetric matrix, the Hermitian inner product becomes real symmetric inner product, i.e., $\langle\Psi|\Phi\rangle = \langle\Phi|\Psi\rangle$, and so on. However, these properties are not always very useful for describing dissipative systems. Since eventually we need to end up with complex eigenvalues representing the frequencies of decaying sinusoids, we have to leave out the Hermiticity property. Interestingly, if we restrict ourselves to the use of complex (non-Hermitian), but symmetric operators and replace the real symmetric inner product by the complex symmetric one, all the relations, that were correct for the real symmetric case will hold. Roughly speaking, this corresponds to an analytic continuation of the real symmetric case in which all the real variables are declared as complex and all the real operations are replaced by complex operations.

Consider an abstract linear vector space $\mathcal{A}$. To distinguish between the Hermitian and complex symmetric inner product for the latter we use the round brackets, $(\Psi|\Phi) = (\Phi|\Psi)$. Note that $(\Psi|\Psi)$ is not necessarily real, i.e., the norm of Ψ is not necessarily defined in our non-Hilbert space. Moreover, $(\Psi|\Psi)$ can even vanish for a nonzero vector Ψ. Although numerically this is unlikely to happen, it is clearly an indication of possible problems (e.g., instability) in the numerical algorithms involving the non-Hermitian inner products.

We will always identify linear operators, $\hat{U}$, $\hat{\Omega}$, etc., that act on vectors in $\mathcal{A}$ by a cap. By the complex symmetric operator $\hat{\Omega}$ we mean that it satisfies the following relationships:

$$\{(\Psi|\}\{\hat{\Omega}|\Phi)\} = \{(\Psi|\hat{\Omega}\}\{|\Phi)\} = (\Psi|\hat{\Omega}|\Phi) \ , \tag{22}$$

for any two vectors $|\Psi)$ and $|\Phi)$ from $\mathcal{A}$. In words, it does not matter whether we first operate with $\hat{\Omega}$ on $|\Phi)$ and then evaluate the inner product with $(\Psi|$ or vice versa.

An operator $\hat{\Omega}$ is diagonalizable, if it has a set of eigenvalues ω_k and eigenvectors $|\omega_k)$ satisfying

$$\hat{\Omega}|\omega_k) = \omega_k|\omega_k) \ , \tag{23}$$

where the eigenvectors are orthonormalized with respect to the complex symmetric inner product, i.e.,

$$(\omega_k|\omega_{k'}) = \delta_{kk'} \ . \tag{24}$$

We will also assume implicitly that our operators are not pathological, which, in particular, means that the eigenvectors form a complete basis and one can use the resolution of identity,

$$\hat{I} = \sum_k |\omega_k)(\omega_k| \ . \tag{25}$$

This also implies that $\hat{\Omega}$ can be expressed using the spectral representation,

$$\hat{\Omega} = \sum_k \omega_k|\omega_k)(\omega_k| \ . \tag{26}$$

The spectral representation becomes very useful when we want to obtain an expression for a function $f(\hat{\Omega})$ of an operator $\hat{\Omega}$, whose eigenvalues and eigenvectors are known:

$$f(\hat{\Omega}) = \sum_k f(\omega_k)|\omega_k)(\omega_k| \ . \tag{27}$$

Note that $f(\hat{\Omega})$ is also an operator with the eigenvalues $f_k = f(\omega_k)$ and the same eigenvectors $|\omega_k)$.

If we now adapt the quantum mechanical terminology by calling $\hat{\Omega}$ a Hamiltonian, the following operator functions will be of most interest, namely, the time evolution operator $\hat{U}(t)$ and the two resolvent operators $\hat{G}(s)$ and $\hat{G}^\tau(s)$, related to $\hat{U}(t)$ via the integral and discrete Fourier transformations according to, respectively, Eqs. 15 and 16. The spectral representations of these operators, according to Eq. 27, are

$$\hat{U}(t) \equiv e^{-it\hat{\Omega}} = \sum_k e^{-it\omega_k}|\omega_k)(\omega_k| \ , \tag{28}$$

$$\hat{G}(s) \equiv \frac{1}{\hat{\Omega} - s} = \sum_k G_k(s)|\omega_k)(\omega_k| \ , \tag{29}$$

$$\hat{G}^\tau(s) \equiv \frac{i\tau}{1 - e^{i\tau(s-\hat{\Omega})}} - \frac{i\tau}{2} = \sum_k G_k^\tau(s)|\omega_k)(\omega_k| \ . \tag{30}$$

Clearly, these operators are complex symmetric as they are some analytic functions of the complex symmetric operator $\hat{\Omega}$.

It is also possible to extend the spectral representation to the case of the imaginary part of an operator,

$$\mathrm{Im}\left\{\hat{\Lambda}\right\} = \sum_k \mathrm{Im}\left\{\lambda_k\right\} |\lambda_k)(\lambda_k| \ , \tag{31}$$

where λ_k and $|\lambda_k)$ are eigenvalues and eigenfunctions of a general operator $\hat{\Lambda}$. It is important to realize that generally $\mathrm{Im}\left\{\hat{\Lambda}_1 + \hat{\Lambda}_2\right\} \neq \mathrm{Im}\left\{\hat{\Lambda}_1\right\} + \mathrm{Im}\left\{\hat{\Lambda}_2\right\}$ if the operators $\hat{\Lambda}_1$ and $\hat{\Lambda}_2$ do not commute, i.e., taking the imaginary part *is not* a linear operation.

With this definition we can introduce the *spectral density* operators

$$\hat{\delta}(s) \equiv \mathrm{Im}\left\{\hat{G}(s)\right\} = \sum_k \delta_k(s)|\omega_k)(\omega_k| \tag{32}$$

$$\hat{\delta}^\tau(s) \equiv \mathrm{Im}\left\{\hat{G}^\tau(s)\right\} = \sum_k \delta_k^\tau(s)|\omega_k)(\omega_k| \ , \tag{33}$$

which will mostly be useful later in the framework of constructing the D-dimensional absorption mode spectra.

For a vector $|0)$, here called the *initial state*, we can consider the vector $|t)$ evolving in time according to

$$|t) = \hat{U}(t)|0) \ . \tag{34}$$

Since $\hat{\Omega}$ is not Hermitian, the evolution operator $\hat{U}(t)$ is not unitary, i.e., its eigenvalues do not necessarily belong to the unit circle in the complex plane. This also implies that the norm of the vector $|t)$ is not preserved, which is the case of a dissipative dynamics.

It is often convenient (although, not necessary) to assume that all the eigenvalues $\omega_k \equiv \nu_k - i\gamma_k$ of $\hat{\Omega}$ have negative imaginary parts, $\gamma_k > 0$, i.e., all the eigenvalues of $\hat{U}(t)$ are inside the unit circle. In this case the time autocorrelation function

$$c(t) = (0|t) \tag{35}$$

will strictly decay in time. This is easy to see if we insert Eq. 34 into Eq. 35 and then use the spectral representation of $\hat{U}(t)$, Eq. 28:

$$\begin{aligned} c(t) &= (0|\hat{U}(t)|0) = \sum_k (0|\omega_k)(\omega_k|0)e^{-it\omega_k} \\ &= \sum_k d_k e^{-it\omega_k} \equiv \sum_k d_k e^{-it\nu_k} e^{-t\gamma_k} \ , \end{aligned} \tag{36}$$

with the amplitudes

$$d_k = (0|\omega_k)^2 \ , \tag{37}$$

defining the projections of the initial state $|0)$ on the eigenvectors $|\omega_k)$. The real number γ_k is naturally called the *width* or *inverse lifetime* of the k-th resonance state.

The set of parameters $\{\omega_k, d_k\}$ corresponds to spectral representation of our quantum dynamical system with the initial state $|0)$. The spectral parameters completely define the time correlation function $c(t)$ due to the relation, Eq. 36.

Another characteristics of our dynamical system defined by $|0)$ and $\hat{\Omega}$ corresponds to the integral or discrete FT spectra. (Note that the infinite time FT exists only if $c(t)$ does not have exponentially increasing components, while the spectral parameters can be defined without this condition.) The two representations are related because using Eq. 36 the Fourier integral (or sum) can be evaluated analytically.

It is useful to express the Fourier spectra $I(s)$ and $I^\tau(s)$ in terms of the matrix elements of the corresponding resolvent operators:

$$I(s) \;=\; (0|\hat{G}(s)|0)\ , \tag{38}$$

$$I^\tau(s) \;=\; (0|\hat{G}^\tau(s)|0)\ , \tag{39}$$

which follows from Eqs. 13,29, and Eqs. 14,30, respectively. Furthermore, for the absorption mode spectra we have

$$A(s) \;=\; (0|\hat{\delta}(s)|0)\ , \tag{40}$$

$$A^\tau(s) \;=\; (0|\hat{\delta}^\tau(s)|0)\ . \tag{41}$$

Note, that the use of $\hat{G}^\tau(s)$ and $\hat{\delta}^\tau(s)$, rather than $\hat{G}(s)$ and $\hat{\delta}(s)$, may be computationally advantageous in the discrete time framework as will be seen below.

Quite amazingly, the time correlation function $c(t)$, Eq. 36, exactly satisfies the form of Eq. 11 so if the $|0)$ and $\hat{\Omega}$ (or $\hat{U}$) are known explicitly, one could convert the HIP to the problem of diagonalizing $\hat{\Omega}$ (or $\hat{U}$). If we were very naive, we would try to diagonalize it by choosing some basis set, say, $\{|\Psi_j)\},\ j = 1, ..., K$, evaluating the matrix elements $[\mathbf{\Omega}]_{jj'} = (\Psi_j|\hat{\Omega}|\Psi_{j'})$ in this basis, and then diagonalizing the $K \times K$ matrix $\mathbf{\Omega}$ in the hope that for large enough K we could converge all the relevant eigenvalues ω_k and eigenvectors $|\omega_k)$. Apparently, this naive idea can be realized by choosing quite a special set of basis vectors which allows one to evaluate the required matrix elements only in terms of the available data, i.e., c_n. This is shown in the next section.

4. HIP CAN BE SOLVED BY PURE LINEAR ALGEBRA.

With the quantum mechanical ansatz (assumption) of the previous section derivation of an eigenvalue problem for the frequencies ω_k and amplitudes d_k that are unknowns in HIP, Eq. 11, becomes very simple. We only need to choose a suitable basis set.

Apparently, instead of the eigenvalue problem for the Hamiltonian $\hat{\Omega}$ [1], it is more convenient to consider equation [2]

$$\hat{U}|\omega_k) = u_k|\omega_k) \tag{42}$$

for the evolution operator $\hat{U} \equiv \hat{U}(\tau) \equiv e^{-i\tau\hat{\Omega}}$ which has eigenvalues $u_k = e^{-i\tau\omega_k}$ with the same eigenvectors $|\omega_k)$. For a sufficiently small τ knowing u_k is equivalent to knowing ω_k. In the following we will try to diagonalize $\hat{U}$.

The initial state $|0)$ belongs to our linear vector space $\mathcal{A}$. According to Eq. 37 $|0)$ has non-zero projections on all the eigenvectors $|\omega_k)$ with weights d_k. An application of $\hat{U}$ to $|0)$ will result in another vector, $|1) = \hat{U}|0)$, from $\mathcal{A}$, that is some other linear combination of the eigenvectors $|\omega_k)$. This way we can generate a subspace of vectors from $\mathcal{A}$,

$$|n) = \hat{U}^n|0), \quad n = 0, ..., M-1\ . \tag{43}$$

We can regard the index n as discrete time. Accordingly, we can consider the discrete time correlation function,

$$c_n = (0|n) = (0|\hat{U}^n|0) \ . \tag{44}$$

Each vector $|n)$ is some linear combination of the eigenvectors $|\omega_k)$ of $\hat{U}$. Such a subspace is called *Krylov subspace* in the theory of linear operators. If M is less than the rank, say K, of $\hat{U}$, these vectors will generally be linearly independent. (Note again that K does not have to be fixed or even finite; neither do we have to use K as a superscript in the summation of Eq. 11.) Thus, we can regard the set $\{|n)\}$ as a basis set. Now consider a particular eigenvector $|\omega_k)$. Assume that for sufficiently large M the following expansion holds,

$$|\omega_k) = \sum_{n=0}^{M-1} [\mathbf{B}_k]_n \, |n), \tag{45}$$

where $\mathbf{B}_k$ defines a column vector with coefficients $[\mathbf{B}_k]_n$. Inserting Eq. 45 into Eq. 42 and multiplying both sides by $(n'|$ from the left we obtain the generalized eigenvalue problem for the eigenvalues u_k and the eigenvectors $\mathbf{B}_k$,

$$\sum_{n=0}^{M-1} [\mathbf{U}_1]_{n'n} \, [\mathbf{B}_k]_n = u_k \sum_{n=0}^{M-1} [\mathbf{U}_0]_{n'n} \, [\mathbf{B}_k]_n \ \ , \tag{46}$$

where we introduced the convenient notation

$$[\mathbf{U}_p]_{n'n} = (n'|\hat{U}^p|n) \tag{47}$$

for the $M \times M$ matrix representation of the operator $\hat{U}^p$ in the Krylov basis. With this notation $\mathbf{U}_0$ is the overlap matrix, which is different from the unit matrix as the Krylov vectors are not orthonormal.

Eq. 46 can also be written in a matrix form,

$$\mathbf{U}_1 \mathbf{B}_k = u_k \mathbf{U}_0 \mathbf{B}_k \ . \tag{48}$$

Quite importantly, the matrix elements of $\mathbf{U}_p$ can be expressed only in terms of the discrete time correlation function, Eq. 44, as

$$[\mathbf{U}_p]_{n'n} = (0|\hat{U}^{n+n'+p}|0) = c_{n+n'+p} \ \ , \tag{49}$$

where we utilized the complex symmetric property of $\hat{U}$, like in Eq. 22, and then recognized Eq. 44. The matrix $\mathbf{U}_p$ can be viewed as a p-independent linear functional of the signal c_n with total length $2M-1$ shifted by p. As such evaluation of Eq. 49 requires the knowledge of c_n for $n = p, p+1, \ \dots \ , p+2M-2$.

Once the frequencies ω_k are known from the solution of Eq. 48, one can solve for the amplitudes d_k by solving the linear least squares equation, Eq. 11, with respect to d_k, as commonly done in other linear algebraic approaches. However, d_k's can also be computed directly using the eigenvectors $\mathbf{B}_k$ [1]. Note first, that because of Eqs. 24 and 45 the eigenvectors $\mathbf{B}_k$ are subject to orthonormalization with respect to the overlap matrix:

$$\mathbf{B}_{k'}^{\mathrm{T}} \mathbf{U}_0 \mathbf{B}_k = \delta_{kk'} \ . \tag{50}$$

Practically, any two eigenvectors, that are solutions of Eq. 48 with different eigenvalues, have to be automatically orthogonal, so only the normalization part of Eq. 50 for each eigenvector has to be implemented. Finally, because of Eqs. 37 and 45, the properly orthonormalized eigenvectors can be used to compute the amplitudes,

$$\sqrt{d_k} = \mathbf{B}_k^{\mathrm{T}} \mathbf{C} \ , \tag{51}$$

where $\mathbf{C} = (c_0, ..., c_{M-1})^{\mathrm{T}}$ is a known $1 \times M$ column vector.

To appreciate the result which we just derived, note that we only assumed c_n to satisfy Eq. 11 with the frequencies ω_k and amplitudes d_k related to the eigenvalues and eigenvectors of $\hat{U}$. The latter is not known, but it is not needed either, as the information, only in terms of the sequence c_n with $n = 0, ..., N-1 = 2M-1$, is sufficient to construct the $\mathbf{U}_1$ and $\mathbf{U}_0$ matrices of size $M \times M$ to be used in Eq. 48 to solve for u_k and $\mathbf{B}_k$.

Eqs. 48-51 constitute a remarkably simple method of solving the HIP, i.e., parametric classification of a time signal c_n. There was no name given to this particular method of parameter estimation in ref. [2]. Here to distinguish it from FDM we call it *Krylov Basis Diagonalization Method* (KBDM).

By deriving the above equations we also proved that a finite signal of size $N = 2M$ can be fitted uniquely by the form of Eq. 11 using $M = N/2$ complex sinusoids, i.e., the N unknowns can be obtained uniquely from N equations. Of course, this observation does not imply that the results are signal size independent. The latter will only be true if a signal has exactly the form of Eq. 11 with some fixed and finite number of terms K, in which case for $N \geq 2K$, i.e., $M \geq K$, the rank of both matrices, $\mathbf{U}_1$ and $\mathbf{U}_0$, will be K. That is, for $M > K$ they will be singular with exactly $M - K$ zero eigenvalues. The non-degenerate subspace (the "range space") of rank K will uniquely define the K frequencies ω_k and K amplitudes d_k.

It must be noted that noiseless signals hardly occur in real life (they can only occur in theory [2]). The singularity of the data matrix is removed by a general small perturbation of the signal. Noise always plays the role of such a perturbation, in which case, roughly speaking, $M - K$ pairs of (ω_k, d_k) with small d_k describe the noise. Obviously, noisier data requires longer signals to achieve the same resolution. However, one should be very careful when interpreting a line list of a noisy signal as it is often impossible to separate the genuine poles from the noise poles due to their interference.

4.1. Example: K=2.

The simplest nontrivial example of a HIP corresponds to having two sinusoids, i.e., consider the signal

$$c_n = d e^{-in\tau(\omega - \Delta\omega)} \ + \ d' e^{-in\tau(\omega + \Delta\omega)} \ , \qquad n = 0, 1, 2..., N-1 = 2M-1 \tag{52}$$

Now we want to set up and solve the KBDM equations to invert c_n using $M = 1$ and $M = 2$.

***M* = 1**

Although we know that with just one basis function one cannot possibly get two eigenvalues, we consider this case as it reveals some interesting properties of the harmonic inversion solutions.

$M = 1$ corresponds to the total signal length $N = 2$. Eq. 48 for this case boils down to the 1×1 generalized eigenvalue problem,

$$c_1 \mathbf{B}_1 = u_1 c_0 \mathbf{B}_1 \ .$$

There is only one eigenvalue

$$u_1 \equiv e^{-i\tau\omega_1} = \frac{c_1}{c_0} = e^{-in\tau\omega}\frac{de^{-i\tau\Delta\omega} + d'e^{i\tau\Delta\omega}}{d+d'} \ . \tag{53}$$

The eigenvector, which is just a number, after the normalization $\mathbf{B}_1 c_0 \mathbf{B}_1 = 1$ (see Eq. 50) is given by

$$\mathbf{B}_1 = 1/\sqrt{c_0} \ .$$

Therefore, the solution for the amplitude (see Eq. 51) is

$$d_1 = \mathbf{B}_1 c_0 = d + d' \ . \tag{54}$$

That is, a single-sinusoid-fit of a sum of two complex sinusoids has an amplitude equal to the sum of the two amplitudes and oscillates with a frequency which is some weighted average of the two underlying frequencies. Eq. 53 implies that even if both genuine frequencies $\omega \pm \Delta\omega$ were purely real, the solution given by ω_1 will be complex, i.e., will have some width of order of $\Delta\omega$ to account for the two peaks separated by $2\Delta\omega$. In other words, the spectrum given by this single Lorentzian line will be of a low resolution type. This simple example demonstrates that even if the problem is underdetermined ($M < K$), the method does not collapse. Also note, that in the $\Delta\omega \to 0$ limit, i.e., the single sinusoid case, Eqs. 53 and 54 recover the exact result as they should.

$\boldsymbol{M = 2}$

The case of two Krylov basis functions requires the use of $N = 4$ signal points and needs the solution of the following 2×2 generalized eigenvalue problem,

$$\begin{pmatrix} c_1 & c_2 \\ c_2 & c_3 \end{pmatrix} \begin{pmatrix} [\mathbf{B}_k]_1 \\ [\mathbf{B}_k]_2 \end{pmatrix} = u_k \begin{pmatrix} c_0 & c_1 \\ c_1 & c_2 \end{pmatrix} \begin{pmatrix} [\mathbf{B}_k]_1 \\ [\mathbf{B}_k]_2 \end{pmatrix} \tag{55}$$

The eigenvalues can be found from the roots of the corresponding secular equation,

$$\det \begin{pmatrix} c_1 - u_k c_0 & c_2 - u_k c_1 \\ c_2 - u_k c_1 & c_3 - u_k c_2 \end{pmatrix} = 0 \ .$$

After substituting the assumed form for the c_n terms, Eq. 52, one can check that the two roots are $u_1 = e^{-i\tau(\omega+\Delta\omega)}$ and $u_2 = e^{-i\tau(\omega-\Delta\omega)}$. Solving then Eq. 55 for the eigenvectors, normalizing them according to Eq. 50,

$$\left([\mathbf{B}_k]_1 \ \ [\mathbf{B}_k]_2 \right) \begin{pmatrix} c_1 & c_2 \\ c_2 & c_3 \end{pmatrix} \begin{pmatrix} [\mathbf{B}_k]_1 \\ [\mathbf{B}_k]_2 \end{pmatrix} = 1 \ ,$$

and using Eq. 51,

$$\sqrt{d_k} = \left([\mathbf{B}_k]_1 \ \ [\mathbf{B}_k]_2 \right) \begin{pmatrix} c_0 \\ c_1 \end{pmatrix} \ ,$$

then recovers the two amplitudes, $d_1 = d$ and $d_2 = d'$.

Thus for a noiseless signal made of two complex sinusoids the spectral parameters can be calculated to essentially machine accuracy using just four signal points, regardless of how close the two frequencies are to each other. This is quite different from the conventional FT spectral analysis which will require a very fine frequency grid (with a spacing less than $\Delta\omega$) and therefore many time-domain points to resolve two very close lines, no matter how high the SNR is. That is, the FT cannot take the full advantage of the high SNR, while in a parametric fit of the signal the sensitivity is naturally converted into high resolution.

It might be useful to check that for $M > K$ (here $K = 2$) the $\mathbf{U}_1$ and $\mathbf{U}_0$ matrices will indeed be singular with $M - K$ zero eigenvalues. Such a case requires a special algorithm (e.g., the QZ-algorithm [44]) which takes care of the singularities, yet, it can be checked that for, e.g., $M = 3$ the corresponding 3×3 generalized eigenvalue problem will have the same $K = 2$ correct eigenvalues, and their two eigenvectors will result in the correct amplitudes.

5. RRT: THE REGULARIZED RESOLVENT TRANSFORM FOR DIRECT SPECTRAL ESTIMATION.

The amplitudes d_k together with frequencies ω_k can be used for spectral estimation according to either Eq. 13 or Eq. 14. Alternatively, due to the resolvent formula, Eq. 39, the infinite time DFT spectrum can be estimated directly (i.e., avoiding the solution of the generalized eigenvalue problem) using the *Resolvent Transform* formula [14]

$$I^\tau(s) = \mathbf{C}^{\mathrm{T}}\mathbf{R}(s)^{-1}\mathbf{C} - \frac{i\tau c_0}{2} \;, \tag{56}$$

where we have defined another data matrix in the form of a *matrix pencil*:

$$\mathbf{R}(s) = \frac{\mathbf{U}_0 - e^{i\tau s}\mathbf{U}_1}{i\tau} \;. \tag{57}$$

(Note, that in place of $\mathbf{R}(s)$ we will often use $\mathbf{R}$ to simplify the notation.)

Rather surprisingly, Eqs. 56 is a working expression. In the case when Eq. 11 is exactly satisfied, it yields the exact infinite time DFT spectrum, if we choose $M = K$, *even though only a finite part of the signal c_n of size $N = 2M$ is used and the spectral parameters ω_k and d_k are not computed.* The result is also exact if $M > K$, although in this case both $M \times M$ U-matrices are singular requiring the use of a pseudo-inverse of $\mathbf{R}$. In practice, the measured data contains some noise, so the matrices are not exactly singular, although they could still be very ill-conditioned, so some kind of regularization will often be required. When calculating $I^\tau(s)$ it might still be a good idea to solve the generalized eigenvalue problem (48) to be able to generate the results for all values of s with no extra cost. However, it is not necessary if a fast linear system (i.e., $\mathbf{R}(s)\mathbf{X}(s) = \mathbf{C}$) solver is available, for instance, if it can take advantage of the special form of the s dependence of the resolvent in Eq. 56 or, more importantly, if it allows one to implement an efficient regularization scheme, which happens to be the case here. (Note that a both robust and computationally efficient regularization of FDM that can be applied to a generic multidimensional signal is still an open problem.)

In what follows we present a brief discussion of regularization for the present context. Much more elaborate discussion on regularization of ill-conditioned linear systems can be found in the tutorial by Neumaier [45].

In order to regularize Eq. 56 one can replace the true inverse $\mathbf{R}^{-1}$ by a pseudo-inverse $\mathbf{R}_q^{-1}$ with some regularization parameter q, arriving at the *Regularized Resolvent Transform* (RRT),

$$I^\tau(s) = \mathbf{C}^{\mathrm{T}}\mathbf{R}_q^{-1}\mathbf{C} - \frac{i\tau c_0}{2} \;. \tag{58}$$

Now one has several options.

5.1. Regularization by Singular Value Decomposition.

SVD of the square $K_{\rm win}\times K_{\rm win}$ matrix $\mathbf{R}$ is defined as

$$\mathbf{R}=\mathbf{W}\mathbf{\Lambda}\mathbf{V}^{\dagger} \tag{59}$$

with unitary $K_{\rm win}\times K_{\rm win}$ matrices $\mathbf{W}$ and $\mathbf{V}$ and real diagonal matrix $\mathbf{\Lambda}=\mathrm{diag}(\lambda_i)$ with $\lambda_1\geq\lambda_2\geq\ldots\geq\lambda_{K_{\rm win}}\geq 0$. Now the problem of regularizing $\mathbf{R}^{-1}$ is reduced to regularization of $\mathbf{\Lambda}^{-1}$, so that we can write

$$\mathbf{R}_q^{-1}=\mathbf{V}\mathbf{\Lambda}_q^{-1}\mathbf{W}^{\dagger} \tag{60}$$

with $\mathbf{\Lambda}_q^{-1}$ defining a pseudo-inverse of $\mathbf{\Lambda}$.

The simplest regularization procedure corresponds to the use of the *truncated SVD*:

$$\left[\mathbf{\Lambda}_q^{-1}\right]_{ii}=\begin{cases}1/\lambda_i\ , & \lambda_i>q\ ,\\ 0\ , & \lambda_i<q\ .\end{cases} \tag{61}$$

Truncated SVD is a very good option in cases when there is a clear threshold q between the subset of nearly singular values $\lambda_i\ll q$ ("the null space") and the other values $\lambda_i\gg q$ ("the range space"). Unfortunately, for realistic signals this is often not the case and there is no general prescription on how to choose q. The results could abruptly depend on q, so the use of this technique is often associated with frustration and subjectiveness. A much better regularization would be, for example,

$$\left[\mathbf{\Lambda}_q^{-1}\right]_{ii}=\frac{\lambda_i}{\lambda_i^2+q^2}\ , \tag{62}$$

in which the "singular" contributions are not removed abruptly.

Although Eq. 62 is a smooth regularization, the main problem associated with it is still the lack of a general prescription on how to choose q. Thus the cheapest and easiest way to both choose optimal q and construct the best solution is to generate the spectra with several values of q. Even though SVD is, generally, quite expensive, the benefit of using it is that the results with different q could be generated at no extra cost.

5.2. Tikhonov Regularization.

Much less numerically expensive, than SVD, is the Tikhonov regularization [41] in which a pseudo-inverse is obtained according to

$$\mathbf{R}_q^{-1}=\left(\mathbf{R}^{\dagger}\mathbf{R}+q^2\right)^{-1}\mathbf{R}^{\dagger}\ , \tag{63}$$

where, again, q plays the role of a regularization parameter. With such a regularization the singularity in the denominator is removed as $\left(\mathbf{R}^{\dagger}\mathbf{R}+q^2\right)$ is a Hermitian and positive definite matrix.

Eq. 58 can now be evaluated by solving the regularized Hermitian least squares problem,

$$\left(\mathbf{R}^{\dagger}\mathbf{R}+q^2\right)\mathbf{X}(s)=\mathbf{R}^{\dagger}\mathbf{C}\ , \tag{64}$$

and then using

$$I^{\tau}(s)=\mathbf{C}^{\mathrm{T}}\mathbf{X}(s)-\frac{i\tau c_0}{2}\ . \tag{65}$$

Although the Tikhonov regularization is much faster than an SVD based regularization, the fact that there is no saving if it is implemented for different values of q, makes it less attractive.

5.3. The status of RRT.

The spectral estimation given by Eqs. 58, 60 and 62 (or Eqs. 64 and 65) has a status of a "transform" (like DFT), while a "method", e.g. the Filter Diagonalization Method, would refer to a procedure that would generally be less obvious to use. More precisely, Eq. 58 corresponds to a direct nonlinear transformation of the time signal to the frequency domain. Unlike most other nonlinear spectral estimators, RRT is very stable with the regularization parameter q controlling both the stability and resolution, whether used in Eq. 62 or 63: a bigger q suppresses the spectral artifacts, decreases the resolution, and therefore leads to a more uniform spectral estimate. These effects occur more smoothly as a function of q than in the truncated SVD approach.

Since RRT approximates the infinite-time DFT, the latter can be replaced by the former. Just like DFT, the RRT, while being amazingly stable and easy to use, has some drawbacks: (i) it is a spectral estimator and as such does not automatically provide one with a line list; (ii) generally, one has difficulties in constructing absorption mode spectra in multidimensional spectral estimation (see below) when a single purely phase modulated data is processed, while in FDM various types of spectra are easily constructed using the computed spectral parameters.

6. FOURIER BASIS FOR LOCAL SPECTRAL ANALYSIS.

Being very simple both KBDM and RRT implemented with Krylov basis of size $M = N/2$ have at least one very serious problem, namely, they scale cubically with respect to the size N of the signal. This means that they cannot be applied, on a regular basis, to signals of size more than, say, a few thousand data points. Fortunately, the problem is not so severe as it seems because there are ways to avoid the global fit of a huge signal by breaking the spectral analysis problem into small windows. In FDM this is done by implementing a Fourier filter [1] to the basis functions. Note that the U-matrices have a very special Hankel structure. There exists a unitary transformation corresponding to certain Fourier basis [2] that can be implemented efficiently. The resulting matrices have much better structure and can be diagonalized in a block fashion.

To be absolutely fair, the idea of making the high resolution spectral analysis local, called *beamspacing* in the engineering literature, has been known for a long time (see, for example, ref. [46]) and has been widely exploited in various contexts. However, to the best of our knowledge, the developed beam space methods are hardly known in the NMR community and are not designed for the specific problems of NMR data processing, although note that a variant of the beam space idea has been implemented in conjunction with LP [47]. The latter method, called LP-ZOOM, has not been used much in the NMR data processing, so there is not enough information to evaluate its performance.

FDM is certainly one of possibly many ways to tackle the problem, but is well tested, robust, computationally efficient and generalizable to the multidimensional case.

To this end, our goal here is, for a given small spectral window, to construct a small set of basis functions that form a locally complete basis. In other words, for an eigenvalue ω_k of $\hat{\Omega}$ inside the specified window, we want the corresponding eigenfunction $|\omega_k)$ to be a linear combination of only a few basis functions. As such consider the discrete Fourier transformation of the Krylov basis,

$$|\varphi_j) = \sum_{n=0}^{M-1} e^{in\tau\varphi_j}|n) \equiv \sum_{n=0}^{M-1} e^{in\tau(\varphi_j-\hat{\Omega})}|0)\ . \tag{66}$$

To remove the ambiguity in the choice of the φ_j values we can consider an equidistant grid,

$$\varphi_j = \frac{2j\pi}{M\tau} \ , \ j = 1, ..., M \ . \tag{67}$$

For this choice the transformation from the Krylov basis $\{|n)\}$, $n = 0, ..., M-1$, to the Fourier basis $\{|\varphi_j)\}$, $j = 1, ..., M$, is unitary. More importantly, each basis function $|\varphi_j)$ is localized in the frequency domain, i.e., it is a linear combination of only those eigenfunctions $|\omega_k)$ of $\hat{\Omega}$ for which $\omega_k \sim \varphi_j$. This can be checked by evaluating the sum in Eq. 66 analytically and using the spectral representation of $\hat{\Omega}$:

$$\begin{aligned} |\varphi_j) &= \frac{1 - e^{iM\tau(\varphi_j - \hat{\Omega})}}{1 - e^{i\tau(\varphi_j - \hat{\Omega})}} |0) \\ &\sim \sum_{\omega_k \sim \varphi_j} \frac{1 - e^{iM\tau(\varphi_j - \omega_k)}}{1 - e^{i\tau(\varphi_j - \omega_k)}})(\omega_k|0)|\omega_k) \ , \end{aligned}$$

and noticing that only a few terms with $\omega_k \sim \varphi_j$ are significantly contributing to $|\varphi_j)$. This also implies that we can consider a small subset of, say, $K_{\text{win}} \ll M$ values φ_j in the frequency region $[\omega_{\min}, \omega_{\max}]$ so that

$$|\omega_k) \approx \sum_{\omega_k \sim \varphi_j} \left[\tilde{\mathbf{B}}_k\right]_j |\varphi_j) \ , \tag{68}$$

where here and throughout the rest of the article the tilde identifies the use of the Fourier basis. Now $\hat{U}$ can be diagonalized in the Fourier subspace corresponding to some prespecified frequency window to yield the eigenvalues and eigenvectors from this window. (Alternatively, the RRT spectrum can be evaluated directly using the resolvent $\hat{G}^\tau(s)$ represented in the same small Fourier basis.) By choosing another window one can obtain another subset of converged eigenvalues and eigenvectors, and so on. Note that the extraction of the eigenfrequencies ω_k to a high precision only requires that the local completeness condition,

$$\rho(\varphi_j) \approx \frac{N\tau}{4\pi} \geq \rho(\omega_k) \ , \tag{69}$$

be satisfied for the density of the grid points φ_j, defined by the information density in the frequency domain contained in the data of size N, and the density of the complex poles ω_k. In other words, the signal length N should be sufficient to justify the use of K_{win} basis vectors $|\varphi_j)$ in the interval $[\omega_{\min}, \omega_{\max}]$ that dominates the number of the eigenvalues ω_k in this interval. The local spectral analysis not only avoids problems of estimating the total rank K of the signal subspace, but, to certain extent, is also insensitive to the spectral properties outside $[\omega_{\min}, \omega_{\max}]$.

The use of a narrow-band basis is the essence of the original Neuhauser's filter diagonalization for extracting the spectra of large Hamiltonian matrices [17], although the form of Eq. 66, as introduced in ref. [2], is both simple and numerically more efficient than the Fourier basis of ref. [1].

To proceed further let us define the matrix elements of $\hat{U}^p$ in the Fourier basis

$$\left[\tilde{\mathbf{U}}_p\right]_{jj'} = (\varphi_j | \hat{U}^p | \varphi_{j'}) \, . \tag{70}$$

Since the vectors $|\varphi_j)$ defined by Eq. 66 are linear combinations of the primitive Krylov vectors $|n)$, the matrix $\tilde{\mathbf{U}}_p$ is a functional of only the $\{c_n\}$ sequence and does not depend explicitly on either of the auxiliary objects $\hat{U}$, ω_k or $|0)$. Inserting Eq. 66 into Eq. 70 for the matrix elements of $\tilde{\mathbf{U}}_p$ and using the result of Eq. 49 we have

$$\left[\tilde{\mathbf{U}}_p\right]_{jj'} = \sum_{n'=0}^{M-1}\sum_{n=0}^{M-1} e^{in\tau\varphi_j} e^{in'\tau\varphi_{j'}} c_{n+n'+p} \ . \tag{71}$$

This double sum can be simplified to a single sum by changing the variables from (n, n') to $(l = n + n', n')$ and then summing over n', which, after some algebra, gives:

$$\begin{aligned}\left[\tilde{\mathbf{U}}_p\right]_{jj'} &= \hat{S} \sum_{\sigma=0,1} \frac{e^{i\sigma[\tau M(\varphi_{j'}-\varphi_j)+\pi]}}{1-e^{i\tau(\varphi_{j'}-\varphi_j)}} \\ &\times \sum_{n=\sigma M}^{(\sigma+1)(M-1)} e^{in\tau\varphi_j} c_{n+p} \ ,\end{aligned} \tag{72}$$

where $\hat{S}$ defines a symmetrization operator over the indices j and j':

$$\hat{S}\ g_{jj'} = g_{jj'} + g_{j'j} \ . \tag{73}$$

Eq. 72 is, in principle, correct for all choices of φ and $\varphi_{j'}$ except for the singularity arising at $\varphi_j = \varphi_{j'}$. To obtain a numerically practical expression for this singular case we evaluate the $\varphi_j \to \varphi_{j'}$ limit leading to

$$\left[\tilde{\mathbf{U}}_p\right]_{jj} = \sum_{n=0}^{2M-2} e^{in\tau\varphi_j}(M - |M-n-1|)c_{n+p} \ . \tag{74}$$

Notably and quite importantly, the resulting matrices $\tilde{\mathbf{U}}_p$ have a sinc-like structure with, as anticipated, generally large diagonal and decaying off-diagonal terms. The latter become much smaller than the former once $M\tau|\varphi_j - \varphi_{j'}| \gg 2\pi$. It is this structure which justifies the possibility of either performing the eigenvalue calculation or the direct spectral estimation by RRT in a small $K_{\rm win} \times K_{\rm win}$ block fashion for possibly large $M \times M$ matrices $\tilde{\mathbf{U}}_p$. Fig. 1 shows the "z-plane" of the evolution operator with its eigenvalues that are assumed to be inside the unit circle. A small frequency window to be used in the FDM calculation is also shown with the region around it where one could expect to obtain the converged eigenvalues.

Using Eqs. 51 and 66 the amplitudes d_k can be easily computed using

$$\sqrt{d_k} = \tilde{\mathbf{B}}_k^{\rm T}\tilde{\mathbf{C}} \ , \tag{75}$$

where the coefficients of the $1 \times K_{\rm win}$ column vector $\tilde{\mathbf{C}}$ are computed using FT of the original $1 \times M$ signal array $\mathbf{C}$:

$$\left[\tilde{\mathbf{C}}\right]_j = \sum_{n=0}^{M-1} e^{in\tau\varphi_j} c_n \ , \quad j = 1, ..., K_{\rm win} \ . \tag{76}$$

7. SPECTRAL ESTIMATION USING THE FDM LINE LIST.

7.1. Multi-window implementation of FDM.

In a single run FDM can obtain results only for a particular small window, in which the most accurate are generally the narrow poles and the ones close to the center of the window. As first noted in ref. [1] in order to describe the overall spectrum one has to implement multiple overlapping windows and throw away the results at the edges of the windows.

In Fig. 2 we show an example of spectral construction by combining the results from several overlapping windows with 50% overlap. For each single window $\left[\omega_{\rm min}^{(r)}, \omega_{\rm max}^{(r)}\right]$ labeled by index r all the frequencies $\omega_k^{(r)}$ and amplitudes $d_k^{(r)}$

are retained and used to construct the spectrum $I^{(r)}(s)$ only inside this window by either Eq. 13 or Eq. 14. The overall spectrum is then constructed by

$$I(s) = \sum_r g^{(r)}(s) I^{(r)}(s) \ , \tag{77}$$

where $g^{(r)}(s)$ is an appropriate weighting function which is non-zero only inside the r-th window $\left[\omega_{\min}^{(r)}, \omega_{\max}^{(r)}\right]$. From our numerical tests we found that any reasonable choice satisfying $\sum_r g^{(r)}(s) = 1$ works well. For example, one can implement

$$g^{(r)}(s) = \frac{1}{2}\left[1 - \cos\left(2\pi \frac{s - \omega_{\min}^{(r)}}{\omega_{\max}^{(r)} - \omega_{\min}^{(r)}}\right)\right] \ , \tag{78}$$

also used in Fig. 2.

Note that in RRT implemented with a Fourier basis [14] the spectra computed for different windows are combined in a similar fashion.

7.2. To flip or not to flip? $I(s)$ or $I^{\tau}(s)$?

The narrow band Fourier basis makes FDM a very powerful tool for high resolution spectral analysis of the time domain data well described by the form of Eq. 11. However, one could wonder if the method is sufficiently stable and robust even when the latter is not the case. To answer this question we can consider the quite simple example of an NMR signal that has a relatively large background spectrum and is relatively noisy (see Fig. 3). As seen in the second trace the FDM ersatz spectrum obtained by Eq. 13 does not reproduce correctly the converged FT spectrum. The reason is that the parameters of very broad poles responsible for the global shape of the noisy baseline cannot be accurately computed when a narrow band Fourier basis is used. The latter works well only for narrow peaks localized in the window, while the non-localized broad spectral features in the presence of noise are not "seen" by the narrow band Fourier basis. Very surprisingly, the same set of ω_k and d_k used with Eq. 14 (the third trace of Fig. 3) reproduces the correct baseline of the DFT spectrum!

Any experienced parameter estimator knows about the subtlety hidden in HIP, Eq. 11, when dealing with non-ideal signals. This subtlety is associated with the possibility to have in the line list a pole $\omega_k \equiv \nu_k - i\gamma_k$ with negative "width", i.e., $\gamma_k < 0$. This formally corresponds to the unphysical exponential increase of the time signal. Since most experimental signals are not ideal one often faces a dilemma on what to do with such a pole? There are several possibilities:

(1) Do nothing.

(2) Flip the unphysical negative γ_k to make it positive and pretend that nothing has happened.

(3) Throw away the unphysical entry with negative γ_k and pretend that nothing has happened.

The first possibility is usually rejected as "obviously wrong" and the choice is made between (2) and (3).

An argument for choice (2) is that if $\gamma_k < 0$ is small, and caused by numerical errors in calculating the width of a very narrow line, the corresponding peak in the absorption spectrum will have the wrong sign. Flipping γ_k then makes the appearance of this peak correct.

An argument for choice (3) is that the entry with negative and large γ_k is spurious and has to be eliminated as there seems to be no reason to keep it.

Once FDM is concerned, we have to take into account the following considerations. When the d_k are computed by solving a least squares problem using Eq. 11 with pre-computed set of the ω_k (as, to the best of our knowledge, is the case for most parameter estimators, but not FDM), an ω_k with negative γ_k can blow up all the amplitudes. Numerical instability is not an issue only if $\gamma_k < 0$ has a small magnitude. Thus, generally, one retains the ω_k with small γ_k flipping the negative γ_k values, while the ω_k with large and negative γ_k values are rejected. The amplitudes d_k together with the frequencies ω_k can then, in principle, be used in Eq. 13 to construct $I(s)$. Unfortunately, the resulting spectrum is often unstable and sensitive to various adjusting parameters. Throwing away a pole ω_k, even if it is not narrow, may lead to a missing peak in the spectrum, while keeping a too broad pole may lead to numerical instabilities. As a consequence, for instance, in most applications of LP, the computed spectral parameters are only used to extrapolate the truncated time signal to somewhat longer times and process it with the conventional DFT.

In FDM the situation is quite different as the amplitudes d_k are computed simultaneously with the frequencies ω_k using, respectively, the eigenvectors and eigenvalues of the generalized eigenvalue problem. Therefore, in FDM $\gamma_k < 0$ does not necessarily lead to any numerical instability in the calculation of the d_k. In our early applications of FDM [2, 7] we always used Eq. 13 to construct the spectrum $I(s)$. As discussed above a narrow peak with negative γ_k will appear upside-down in the absorption spectrum, which is easily fixed by flipping the sign of γ_k. However, because of the local nature of the Fourier basis, which is manifestly incomplete, some computed pairs (ω_k, d_k) may have large and negative γ_k with large d_k values. Those entries would often result in a noticeable baseline distortion when used with Eq. 13 as shown in Fig. 3. Neither throwing away such a "spurious" entry nor flipping the γ_k would fix the baseline. In the spirit of the LP applications it is possible to correct the FDM imperfections in the construction of $I(s)$ by using hybrid methods [1, 11] in which, for instance, narrow poles produced by FDM are retained, while the residual time signal, $\tilde{c}_n = c_n - \sum_k d_k e^{-in\tau\omega_k}$, that contains only rapidly decaying components, is processed by DFT. This, however, does not allow one to obtain a consistent line list. Furthermore, The hybrid methods are not easy to generalize to the multidimensional case where the spectral construction appears to be a very difficult problem. A much more consistent approach is to use a global basis [11] that, in addition to the narrow band Fourier basis describing a narrow frequency domain in high resolution, contains a broad band "coarse" basis vectors covering much broader spectral region (see Fig. 4). Such a *multiscale* basis still has a small overall size while being able to produce a line list $\{\omega_k, d_k\}$ with no spurious entries of the type described above. Such a line list when used in Eq. 13 leads to a stable result.

The unexpected finding shown in the third trace of Fig. 3, that Eq. 14 with the line list $\{\omega_k, d_k\}$ containing some "spurious" entries leads to the correct spectrum with undistorted baseline, can be explained by the fact that it is the $I^\tau(s)$, not $I(s)$, which is invariant to the basis set representation. Due to the existence of very delicate interferences and cancellations of the contributions with large values of both d_k and γ_k in Eq. 14 the instabilities do not occur if one keeps all the entries produced by FDM when using Eq. 14. This also explains the stability of the RRT which relies on the same infinite-time DFT based expression. Clearly, if Eq. 14 gives the correct baseline in the presence of such poles, Eq. 13 must fail as the two expressions are quite different for large γ_k. Consequently, when possible

- *The spectral estimation should be done using the discrete-time expression, Eq. 14.*
- *All the poles with significant amplitudes d_k must be retained in the sum.*
- *Only narrow poles with $\gamma_k < 0$ should be flipped: $\gamma_k \to -\gamma_k$.*

Even though the spectrum is correct, the corresponding broad poles with negative γ_k and large d_k do not correctly describe the time domain data. Therefore, for obtaining a line list consistent with the decaying time signal and with minimized cancellation effects the use of Multiscale FDM is advantageous.

7.3. Multiscale Fourier basis.

Our goal here is for a given small spectral window to construct a sufficiently small basis, which is not only locally complete for the narrow poles inside the window, but also adequately describes the non-localized spectral features. Roughly speaking, the basis should allow us to look at the whole spectrum in a low resolution and, simultaneously, zoom into the chosen small spectral region. A narrow band Fourier basis does not satisfy this criterion. However, one can extend the local basis set to a non-local one by adding appropriate coarse basis functions with wide bandwidth that are capable of describing the overall spectrum at low resolution [11].

There are several ways to introduce a coarse basis. The most straight forward is to use the Krylov vectors $|n)$ up to $n = M_c$ that are added to the narrow band Fourier basis vectors for each single window calculation. Clearly, this method would be applicable only if M_c does not have to be bigger than, say, 10^2. That is, the Krylov type coarse basis is generally applicable to relatively small data sets with relatively simple spectra.

A more consistent strategy is to implement a multiscale Fourier basis by considering a non-uniform distribution of the φ_j and allowing the M in Eq. 66 to be a function of j, essentially defined by the local density $\rho(\varphi_j)$ of φ_j's,

$$M_j = \frac{2\pi}{\tau}\rho(\varphi_j) \ . \tag{79}$$

Thus, for a multiscale Fourier basis Eq. 66 is rewritten as

$$|\varphi_j) = \sum_{n=0}^{M_j-1} e^{in\tau\varphi_j}|n) \ , \ j = 1, ..., K_c + K_{\text{win}} \ , \tag{80}$$

where $K_c + K_{\text{win}}$ is the total size of the basis including both the coarse and narrow band Fourier basis vectors for a given small spectral window. An example of such a non-uniform distribution of the basis vectors in the frequency domain is shown in Fig. 4.

The matrix elements of $\hat{U}^p$ between any two basis functions $|\varphi_j)$ and $|\varphi_{j'})$ can be evaluated (see ref. [11] for detail) leading to

$$\begin{aligned}\left[\tilde{\mathbf{U}}_p\right]_{jj'} &= \hat{S}\sum_{\sigma=0,1}\frac{e^{i\tau\sigma[M_{j'}(\varphi_{j'}-\varphi_j)+\pi]}}{1-e^{i\tau(\varphi_{j'}-\varphi_j)}} \\ &\times \sum_{n=\sigma M_{j'}}^{\sigma(M_{j'}-1)+M_j-1} e^{in\tau\varphi_j}c_{n+p}\end{aligned} \tag{81}$$

for $j \neq j'$ and the diagonal matrix elements defined by Eq. 74. Note that if $M_j = M_{j'}$, Eq. 81 becomes equivalent to Eq. 72, as it should.

The most simplified implementation of a multiscale Fourier basis would correspond to using just two scales, i.e., $M = N/2$ and $M_c \ll M$ where N is the signal size available, with the two equidistant grids of values $\{\varphi_j^{(c)}\}$, $j = 1, ..., K_c$, and $\{\varphi_j\}$, $j = 1, ..., K_{\text{win}}$. Note that some contraction of the coarse basis is possible by simply retaining only those vectors $|\varphi_j)$ for which a low resolution Fourier spectrum is greater than some prespecified threshold value.

Finally, we note that the total size of the coarse basis set can significantly be reduced by a contracting procedure in which FDM is first applied to a short signal with size $2M_c$ and some large spectral window that includes the small window of interest. After Eq. 48 is solved, only those eigenvectors $\tilde{\mathbf{B}}_k^{(c)}$ are retained for which the amplitudes $d_k^{(c)}$ are larger than some prespecified threshold value. These eigenvectors are then added to the narrow band Fourier basis and Eq. 48 is solved again. Clearly, this procedure can be implemented in a "renorm group" fashion, if one wants to make it very complicated.

More detail about the Multiscale FDM with some numerical examples can be found in ref. [11].

7.4. Cheating or resolution enhancement.

Needless to say, the spectral representation of the line list is much simpler and more appealing than the table format, especially, to a visually oriented person. It is difficult for a human operator to analyze the line list which contains many entries with broad and narrow poles with high and low amplitudes, etc. However, the line list contains much more information than the conventional spectrum. For example, some spectral lines are not necessarily singlets, they just happened to appear as singlets because the underlying peaks are broad and strongly overlap. It should be emphasized that the ersatz spectrum of Eq. 14 is just one possible representation of the line list. Of course, it is a very special representation as it estimates the infinite time Fourier sum of c_n. In the framework of the Fourier spectral analysis it is possible to achieve some resolution enhancement by implementing aggressive filters, such as the "pseudo-echo" [40] that could improve the resolution of the peaks at the expense of severe distortion of their amplitudes and enhancement of the noise artifacts. Once we believe that the spectral peaks are Lorentzians, even if they overlap, we can construct another spectral representation of the line list using, e.g., Eq. 14 but with the Lorentzians narrower by some factor [7], $1/\text{cheat} > 1$,

$$\omega_k \equiv \nu_k - i\gamma_k \rightarrow \nu_k - i \cdot \text{cheat} \cdot \gamma_k \ . \tag{82}$$

We call this spectral representation *cheating* as it may lead to wrong conclusions in cases of non-Lorentzian lineshapes, where a single peak would be represented by several interfering Lorentzians. Typical values of the parameter "cheat" are between 0.1 and 1. (Note that for cheat $= 1$ Eq. 82 the widths are unchanged.) Even when the Lorentzian assumption is adequate a too aggressive cheating may lead to significant distortions of the baseline as the amplitudes d_k of the overlapping Lorentzians may be complex. Some ambiguity of the individual amplitudes does not affect the appearance of the spectrum due to the mutual cancellations of the overlapping Lorentzians in Eq. 14, while it may cause significant spectral distortions in Eq. 82, especially because of the non-zero $\mathrm{Im}\{d_k\}$ leading to the dispersion lineshapes. Thus to improve the appearance of the enhanced spectrum Eq. 19 can be implemented, instead of Eqs. 14 and 17, to reinforce the pure absorption lineshapes and then using either $|A^\tau(s)|$ or $\mathrm{Re}\,\{A^\tau(s)\}$ for a real-valued absorption mode spectrum.

Interestingly, unlike the resolution enhancement methods based, for instance, on the sine-bell weighting of the time signals, *cheating* preserves the peak weights since they are defined by the amplitudes, d_k, which are unaffected, and not by the widths.

Fig. 5 shows an interesting part of a proton NMR spectrum of a fluorinated ribose derivative. The overall spectral width was 10 kHz and the size of the signal $N = 8192$ (see ref. [5] for more detail). Both FFT (not shown) and FDM spectra are absolutely converged in the sense that further increase of N does not improve the resolution. The use of Eq. 82 with cheat $= 0.2$ allows us to uncover some splittings, hidden in the conventional spectral representation. The peaks, appearing in the latter as singlets, turn out to be doublets. However, one should always be cautious when trying to interpret such a result, as there is no guarantee that the splittings are real and not caused by the ambiguity of the Lorentzian fit of non-Lorentzian lines.

7.5. Phase correction.

Due to various reasons the first few data points may be corrupted or missing resulting in both the phase and amplitude distortions in the calculated spectra. Therefore, construction of an absorption spectrum requires to correct the distorted phase. If only a couple of data points are missing this can be usually done quite reliably by a linear phase correction of the FT spectrum. However, for long time delays the usual linear phase correction routines cannot eliminate the "phase roll" to flatten the baseline. The usual LP approach to the problem is to first "backward predict" the corrupted time domain data points from the uncorrupted data and then compute the FT spectrum.

Given a line list $\{\omega_k, d_k\}$, another approach (see, e.g., ref. [48, 28]) may be to assume that each frequency ω_k describes a well converged narrow Lorentzian line with amplitude d_k that has a wrong phase. These phases can then be set to zero, i.e.,

$$d_k \longrightarrow |d_k| \ . \tag{83}$$

Note, however, that such a phase correction is very dangerous in cases of either strongly overlapping lines or non-Lorentzian lineshapes or both, when a particular lineshape could be a result of interference and mutual cancellations of many Lorentzians. A much less aggressive procedure based on the same assumption that all amplitudes d_k must be positive is to use Eq. 19 with $|A^\tau(s)|$ to approximate the absorption spectrum. However, this approach cannot be applied for a general case when the amplitudes may have different signs. Here we discuss how the time delay correction can be carried out more consistently in the frame of FDM [7]. Let $\Delta\tau$ be the time delay, corresponding to the first point of the time signal used, i.e.,

$$c_n = c[(n+\Delta)\tau] \ , \ n = 0, ..., N-1 \ . \tag{84}$$

When the HIP, Eq. 11, is solved for such a signal, ideally, the extracted frequencies ω_k should not be affected by the time delay, while the amplitudes $d_k(\Delta\tau) = d_k e^{-i\Delta\tau\omega_k}$ will be modulated by the frequency-dependent factors. Therefore, to correct an extracted amplitude $d_k(\Delta\tau)$ one can simply use the expression

$$d_k = d_k(\Delta\tau) e^{i\Delta\tau\omega_k} \ . \tag{85}$$

Such a correction will be accurate if both the extracted frequency ω_k and amplitude $d_k(\Delta\tau)$ are reliable, which under certain conditions is the case. However, one should realize that the correction factor $e^{i\Delta\tau\omega_k}$ can easily be very large if the width $\gamma_k = -\mathrm{Im}\{\omega_k\}$ of the k-th pole is large. In such a case a small number, $d_k(\Delta\tau)$, is multiplied by a huge number, $e^{i\Delta\tau\omega_k}$, leading to numerical instabilities. The errors of the calculated spectral parameters, ω_k and $d_k(\Delta\tau)$, are not the only source of instability, because the line list obtained by FDM does not only represent the true spectrum. In fact, there always are some noise poles, whose phase correction does not make much sense. Moreover, the widths of the noise poles are not necessarily small, so their time delay "correction" may result in huge baseline distortions. The time delay correction works only if such poles can be identified and removed from the further analysis, for instance, by using a cutoff parameter for γ_k. The problem will occur when such a separation of the signal from noise is not possible.

To this end Eq. 85 has certain limitations. That is, FDM will be a perfect method for correcting the phases distorted by possibly very long time delays but only for lines with Lorentzian lineshapes that are not too broad and do not overlap too strongly with other lines.

Note also, that the said instability in the spectral estimation using the corrected line list can be suppressed by FDM averaging as was done in ref. [7]. We will discuss the averaging procedure in Section 10.1 in a more general framework of multidimensional spectral construction, where numerical instability is the rule rather than an exception.

Finally, we demonstrate here that the spectrum itself can be corrected in the framework of RRT avoiding reference to the line list and, therefore, avoiding some instability problems of the line list correction. This can be done by inserting the time delay evolution operator $\hat{U}^{-\Delta}$ in the expression for the uncorrected spectrum (e.g., Eq. 39):

$$\begin{aligned} I^{\tau}(s) &= (0|\hat{G}^{\tau}(s)\hat{U}^{-\Delta}|0) \\ &\equiv (0|\left\{\frac{i\tau}{\hat{U}^{\Delta} - e^{i\tau s}\hat{U}^{1+\Delta}} - \frac{1}{2\hat{U}^{\Delta}}\right\}|0)\ , \end{aligned} \tag{86}$$

where the second term shifts the spectrum only by a frequency independent constant and is not essential. For integer Δ the numerical implementation of this expression by RRT requires evaluation of the matrices of the operators $\hat{U}^{\Delta}$ and $\hat{U}^{1+\Delta}$ using equations 72 and 74. Some preliminary results obtained using this approach are very encouraging [49], showing that it overperforms FDM in its robustness. A reason for the stability of the time delay correction based on Eq. 86 is the absence of the diverging terms associated with back extrapolation of rapidly decaying signals.

7.6. Reference deconvolution.

Reference deconvolution is a powerful addition to FDM. The first weakness an experimentalist notices with Eq. 11 is the assumption of a Lorentzian lineshape. This is important to the algorithm as a Lorentzian line can be fit by a single entry (d_k, ω_k), while a non-Lorentzian line has to be fit by more than one interfering entries, reducing the efficiency of the FDM. In an NMR experiment the Lorentzian lineshapes may be distorted by either the magnetic field inhomogeneities caused by an imperfectly shimmed magnet, or chemical exchange, or other dynamic processes. In ref. [50] Morris introduced the idea of *reference deconvolution* implemented in the case of inhomogeneous broadening which is unique over the whole spectrum and which corresponds to convolution of the undistorted spectrum with some unknown function. Due to the convolution theorem this is equivalent to the assumption that the measured FID $C_{\rm exp}(t)$ is a product of the perfect FID $C_{\rm exact}(t)$ and some unknown smooth instrumental function of time $f(t)$, plus some experimental noise $y(t)$,

$$C_{\rm exp}(t) = C_{\rm exact}(t)f(t) + y(t)\ . \tag{87}$$

As suggested in ref. [50] the instrumental function f(t) can be obtained by analyzing an isolated reference line such as TMS whose exact lineshape, e.g., in terms of the parameters $\{d_k^{\rm exact}, \omega_k^{\rm exact}\}$, is known. In the frame of FDM this can be realized by processing the measured data and retaining only the entries $\{d_k^{\rm exp}, \omega_k^{\rm exp}\}$ that represent the distorted reference line:

$$f(t) = \frac{C_{\rm exp}^{\rm TMS}(t)}{C_{\rm exact}^{\rm TMS}(t)} = \frac{\sum_k d_k^{\rm exp} e^{-it\omega_k^{\rm exp}}}{\sum_k d_k^{\rm exact} e^{-it\omega_k^{\rm exact}}}\ . \tag{88}$$

Then simply dividing the full FID by f(t) accomplishes the desired deconvolution of the signal,

$$C_{\rm deconv}(t) = C_{\rm exp}(t)/f(t) = C_{\rm exact}(t) + y(t)/f(t)\ . \tag{89}$$

Apparently, even when we know $f(t)$ it is impossible to exactly uncover $C_{\rm exact}(t)$ due to the noise term. Moreover, since $f(t)$ is typically an exponentially decaying function of time and $y(t)$ does not decay, the term $y(t)/f(t)$ exponentially increases in time. That is $C_{\rm deconv}(t)$ has a noisy exponentially increasing tail, which makes the problem non-trivial. for example the Fourier integral of such a signal diverges, while an attempt to regularize the Fourier integral by apodization would contradict the deconvolution idea. At the same time, processing the deconvoluted signal $C_{\rm deconv}(t)$ by FDM will result in a line list $\{d_k^{\rm deconv}, \omega_k^{\rm deconv}\}$ with both negative and positive $\gamma_k = -{\rm Im}\{\omega_k\}$. The latter represent the correct deconvoluted lines, while the former represent the exponentially amplified noise that can be sorted out. (For more detail see ref. [7])

8. MULTIDIMENSIONAL FDM: A "NAIVE" APPROACH.

8.1. Multi-dimensional versus one-dimensional spectral analysis.

After the previous section, one can safely conclude that the theory of 1D FDM with the addition of the 1D RRT is essentially worked out and there might only be some secondary problems left for future studies. This is not the case for multidimensional FDM, although it might appear that the latter is a straightforward extension of the 1D method. The difficulties arise in both areas, the problem of obtaining a meaningful line list and spectral construction. While generally working (but often time consuming) solutions are found for the latter problem, the former still lacks good ideas.

A 2D case might seem to be simpler than a general D-dimensional case, but due to the vector notations the latter requires just a minor modification of the former. Thus, we start by introducing a general complex valued D-dimensional time signal $c_{\vec n} \equiv c(n_1\tau_1, n_2\tau_2, \ldots, n_{\rm D}\tau_{\rm D})$, where $\vec n$ is the time vector, defined on an equidistant rectangular time grid of size $N_{\rm total} = N_1 \times N_2 \times \ldots \times N_{\rm D}$.

The total number of the experimental points, $N_{\rm total}$, is only limited by the instrument time and computer disk capacity and does not usually exceed a gigabyte of data. While the number of the running time points N_1 (we use this convention as it is more convenient for multidimensional signals) may include many points (say, of the order of $N_1 \sim 10^3 - 10^4$), the number of time points in each of the other dimensions is a strictly limited by the total experiment time, and so is usually far fewer.

The original formulation of multidimensional FDM [3, 6, 8] is applicable only to signals with high SNR. However, since it is a very straightforward generalization of the ideas and equations of the 1D FDM, we briefly present it here before describing a more robust but complicated approach.

8.2. D-dimensional FDM.

A fully integrated D-dimensional HIP, can be defined as the following parametric fit of the full D-dimensional data set $c_{\vec n}$,

$$c_{\vec n} = \sum_{k=1}^{K} d_k e^{-i\vec n\vec\omega_k} \equiv \sum_{k=1}^{K} d_k \prod_{l=1}^{\rm D} e^{-i n_l \tau_l \omega_{lk}} \ , \tag{90}$$

where $\vec\omega_k \equiv (\omega_{1k}, \omega_{2k}, \ldots, \omega_{{\rm D}k})$ are vectors of unknown complex frequencies, $\omega_{lk} = \nu_{lk} - i\gamma_{lk}$, and d_k, unknown complex amplitudes. The total number of unknown complex parameters in the D-dimensional line list $\{\vec\omega_k, d_k\}$ with K entries is, therefore, $(D+1)K$.

Generally speaking, Eq. 90 corresponds to a non-linear optimization problem. However, just like the 1D HIP (11), it can be cast into a linear algebraic problem or, more precisely, a family of generalized eigenvalue problems. Again, similarly to the 1D case, K is not an adjusting parameter but rather defined by $N_{\rm total}$, the information content of the signal $c_{\vec{n}}$. Moreover, since the spectral analysis is performed locally, $N_{\rm total}$ unambiguously defines the average local density of spectral features used to fit the data locally in the frequency domain.

A complete line list $\{\vec{\omega}_k, d_k\}$ can be used for spectral estimation. For example, the D-dimensional complex DFT spectrum,

$$I^{\tau}(s_1,...,s_{\rm D}) \;=\; \sum_{\substack{n_l=0\\ l=1,\dots,{\rm D}}}^{\infty} \left\{ \prod_{l=1}^{\rm D} (i\tau_l) \left(1-\frac{\delta_{n_l 0}}{2}\right) e^{in_l\tau_l s_l} \right\} c_{\vec{n}} \tag{91}$$

is estimated by analytic evaluation of the infinite-time DFT of $c_{\vec{n}}$ represented by Eq. 90:

$$I^{\tau}(s_1,...,s_D) = \sum_k d_k \prod_{l=1}^{\rm D} G_{lk}^{\tau_l}(s_l) \tag{92}$$

with $G_{lk}^{\tau_l}(s_l)$ defined by ω_{lk} as in Eq. 16. Apparently, a D-dimensional absorption mode spectrum cannot be derived from a single complex spectrum $I^{\tau}(s_1,...,s_D)$, no matter whether the amplitudes are all phased or not. It is though representable in terms of the line list:

$$A^{\tau}(s_1,...,s_D) = \sum_k d_k \prod_{l=1}^{\rm D} \delta_{lk}^{\tau_l}(s_l) \tag{93}$$

with $\delta_{lk}^{\tau_l}(s_l) = {\rm Im}G_{lk}^{\tau_l}(s_l)$.

Generalization of the 1D quantum ansatz, Eq. 44, is as straightforward as writing the signal in the form of the D-dimensional quantum autocorrelation function,

$$c_{\vec{n}} = (0|\vec{n}) \ , \tag{94}$$

where the Krylov vectors are

$$|\vec{n}) = \hat{U}(\vec{n})|0) \tag{95}$$

and the multi-time evolution operator,

$$\hat{U}(\vec{n}) \equiv \prod_{l=1}^{\rm D} \hat{U}_l^{n_l} \equiv \prod_{l=1}^{\rm D} e^{-i\tau_l n_l \hat{\Omega}_l} \ , \tag{96}$$

corresponding to a set of D commuting complex symmetric Hamiltonians $\hat{\Omega}_l$. For the associated evolution operators $\hat{U}_l = e^{-i\tau_l n_l \hat{\Omega}_l}$ we can write:

$$\hat{U}_l|\omega_{lk}) = u_{lk}|\omega_{lk}) \ , \quad l = 1,...,{\rm D} \ , \tag{97}$$

with the eigenvalues $u_{lk} = e^{-i\tau_l\omega_{lk}}$. In the "naive" approach we assume that (i) there are no degenerate eigenvalues so that the eigenvectors $|\omega_{lk})$ are uniquely defined and (ii) the eigenvectors can be reordered so that $|\omega_{lk}) = |\omega_{1k})$, i.e., $\{|\omega_{1k})\}$ is simultaneously the eigenbasis of all the evolution operators $\hat{U}_l$. With these assumptions the quantum multi-time autocorrelation function of Eq. 94 satisfies the form of the D-dimensional HIP, Eq. 90, with $d_k = (0|\omega_{1k})^2$ (compare with Eq. 37).

Just like in the 1D case, the U-matrices are available in the Krylov basis:

$$[\mathbf{U}_{\vec{p}}]_{\vec{n}'\vec{n}} \equiv (\vec{n}'|\hat{U}(\vec{p})|\vec{n}) = c_{\vec{n}+\vec{n}'+\vec{p}} \ . \tag{98}$$

Thus the signal $c_{\vec{n}}$ with $N_l = 2M_l$ points in the l-th dimension will correspond to the Krylov basis of size $M_{\rm Krylov} = M_1 \times M_2 \times ... \times M_{\rm D} = N_{\rm total} \times 2^{-{\rm D}}$. Now assuming the eigenfunctions $|\omega_{lk})$ can be expanded in the Krylov basis,

$$|\omega_{lk}) = \sum_{\substack{n_r=0\\ r=1,\dots,{\rm D}}}^{M_r} [\mathbf{B}_{lk}]_{\vec{n}} \, |\vec{n}) \ , \tag{99}$$

we can convert the D operator eigenvalue problems, Eq. 97, into D matrix generalized eigenvalue problems,

$$\mathbf{U}_l \mathbf{B}_{lk} = u_{lk} \mathbf{U}_0 \mathbf{B}_{lk} \ , \quad l = 1, ..., {\rm D} \ , \tag{100}$$

where $\mathbf{U}_l$ for $l \geq 1$ is the matrix representation of $\hat{U}_l$ and $\mathbf{U}_0$, the overlap matrix. The orthonormality of $|\omega_{lk})$ implies the orthonormalization condition for the eigenvectors of Eq. 100:

$$\mathbf{B}_{lk'}^{\rm T} \mathbf{U}_0 \mathbf{B}_{lk} = \delta_{kk'} \ . \tag{101}$$

The eigenvalues in Eq. 100 yield the frequencies ω_{lk} and the normalized eigenvectors, the amplitudes,

$$\sqrt{d_k} = \mathbf{B}_{lk}^{\rm T} \mathbf{C} \ , \tag{102}$$

where we used matrix notation for the $M_1 \times ... \times M_{\rm D}$ part of the signal array $\mathbf{C}$ with elements $c_{\vec{n}}$, which makes Eq. 102 look very similar to Eq. 51 used in the 1D case.

If the Krylov basis $\{|\vec{n})\}$ is complete, i.e., Eq. 99 holds, Eq. 100 for different l will result in the same set of eigenvectors $\mathbf{B}_{lk} = \mathbf{B}_{1k}$. This, in particular, means that, theoretically, only one of the D generalized eigenvalue problems has to be solved for the eigenvectors: all the required eigenvalues can then be evaluated using

$$u_{lk} = \mathbf{B}_{1k}^{\rm T} \mathbf{U}_l \mathbf{B}_{1k} \ . \tag{103}$$

One can generate a model signal $c_{\vec{n}}$ by evaluating Eq. 90 using some prespecified set of spectral parameters, $\{\vec{\omega}_k \equiv (\omega_{1k}, ..., \omega_{{\rm D}k}), d_k\}$, $k = 1, ..., K$, and check that the method works, at least in principle: when the condition $M_{\rm Krylov} = N_{\rm total} \times 2^{-{\rm D}} \geq K$ (i.e., the basis size is greater than the rank of the operators $\hat{U}_l$) is satisfied, the spectral parameters can be recovered to many significant digits by solving Eq. 100 (see an example in ref. [3]).

8.3. Solution of the D-dimensional HIP locally in the frequency domain using a Fourier basis.

Clearly, solving Eq. 100 in the Krylov basis is unfeasible for any reasonable size D > 1 NMR signal as $M_{\rm Krylov} = N_{\rm total} \times 2^{-{\rm D}}$ will be too large. Thus, here the local spectral analysis is not an option but a necessity. A D-dimensional Fourier basis is constructed by a straightforward generalization of Eq. 80. Although the advantage of using a multiscale basis over the single-scale one has not been demonstrated yet for a more than 1-dimensional case, we use it here as it is more generic:

$$|\varphi_j) = \sum_{\substack{n_r=0\\ r=1,\dots,{\rm D}}}^{M_{rj}-1} e^{i\vec{n}\vec{\varphi}_j} |\vec{n}) \tag{104}$$

with $\vec{\varphi}_j \equiv (\varphi_{1j}, ..., \varphi_{\mathrm{D}j})$, $j = 1, ..., K_{\mathrm{c}} + K_{\mathrm{win}}$, and $M_{rj} = 2\pi/\rho(\varphi_{rj})$ being a function of the local density at φ_{rj}, $r = 1, ..., \mathrm{D}$. With an appropriate choice for the grid points $\vec{\varphi}_j$ the total sizes K_{win} and K_{c} of, respectively, the window and coarse bases can both be small. A simple and numerically efficient setup could correspond to having two direct-product D-dimensional grids: $\{\vec{\varphi}_j \equiv (\varphi_{1j_1}, ..., \varphi_{\mathrm{D}j_{\mathrm{D}}})\}$, $j_r = 1, ..., K_{r\mathrm{win}}$, with total size $K_{\mathrm{win}} = K_{1\mathrm{win}} \times ... \times K_{\mathrm{Dwin}}$, and $\left\{\vec{\varphi}_j^{(\mathrm{c})} \equiv \left(\varphi_{1j_1}^{(\mathrm{c})}, ..., \varphi_{\mathrm{D}j_{\mathrm{D}}}^{(\mathrm{c})}\right)\right\}$, $j_r = 1, ..., K_{r\mathrm{c}}$, with total size $K_{\mathrm{c}} = K_{1\mathrm{c}} \times ... \times K_{\mathrm{Dc}}$. In each dimension two independent 1D grids of values $\{\varphi_{rj_r}\}$, $j_r = l, ..., K_{r\mathrm{win}}$, and $\left\{\varphi_{rj_r}^{(\mathrm{c})}\right\}$, $j_r = 1, ..., K_{r\mathrm{c}}$ have to be implemented, corresponding to the narrow band Fourier basis with $M_{rj} = M_r$ and coarse basis with $M_{rj} = M_{r\mathrm{c}}$, $M_{r\mathrm{c}}$ being generally much smaller than the maximum allowed order $M_r = N_r/2$ of the Krylov basis in the r-th dimension, dictated by the signal length N_r in this dimension.

The numerical expressions for the matrix elements of $\tilde{\mathbf{U}}_l$, $l = 0, ..., \mathrm{D}$ in the D-dimensional multiscale Fourier basis are obtained by using the 1D result of Eq. 81:

$$\begin{aligned}\left[\tilde{\mathbf{U}}_{\vec{p}}\right]_{jj'} &= \sum_{\substack{\sigma_r=0,1\\ r=1,\ldots,\mathrm{D}}} \left\{\prod_{r=1}^{\mathrm{D}} \hat{S}_r \frac{e^{i\tau_r\sigma_r[M_{rj'}(\varphi_{rj'}-\varphi_{rj})+\pi]}}{1-e^{i\tau_r(\varphi_{rj'}-\varphi_{rj})}}\right\} \\ &\times \sum_{\substack{n_r=\sigma_r M_{rj'}\\ r=1,\ldots,\mathrm{D}}}^{\sigma_r(M_{rj'}-1)+M_{rj}-1} e^{i\vec{n}\vec{\varphi}_j} c_{\vec{n}+\vec{p}}\ ,\end{aligned} \tag{105}$$

where $\hat{S}_r$ defines the symmetrization operator over the subscripts rj and rj' as in Eq. 73. The matrix elements corresponding to $\varphi_{rj} = \varphi_{rj'}$ are computed according to Eq. 74. For example, for $\varphi_{1j} = \varphi_{1j'}$ we have

$$\begin{aligned}\left[\tilde{\mathbf{U}}_{\vec{p}}\right]_{jj'} &= \sum_{\substack{\sigma_r=0,1\\ r=2,\ldots,\mathrm{D}}} \left\{\prod_{r=2}^{\mathrm{D}} \hat{S}_r \frac{e^{i\tau_r\sigma_r[M_{rj'}(\varphi_{rj'}-\varphi_{rj})+\pi]}}{1-e^{i\tau_r(\varphi_{rj'}-\varphi_{rj})}}\right\} \\ &\times \sum_{n_1=0}^{2M_{1j}-2} (M_{1j} - |M_{1j} - n_1 - 1|) \\ &\times \sum_{\substack{n_r=\sigma_r M_{rj'}\\ r=2,\ldots,\mathrm{D}}}^{\sigma_r(M_{rj'}-1)+M_{rj}-1} e^{i\vec{n}\vec{\varphi}_j} c_{\vec{n}+\vec{p}}\end{aligned} \tag{106}$$

with similar expressions to treat other singularities. Finally, for $\vec{\varphi}_j = \vec{\varphi}_{j'}$, i.e., the diagonal elements of the U-matrices, we have

$$\left[\tilde{\mathbf{U}}_{\vec{p}}\right]_{jj} = \sum_{\substack{n_r=0\\ r=1,\ldots,\mathrm{D}}}^{2M_{rj}-2} \left\{\prod_{r=1}^{\mathrm{D}} (M_{rj} - |M_{rj} - n_r - 1|)\right\} e^{i\vec{n}\vec{\varphi}_j} c_{\vec{n}+\vec{p}} \tag{107}$$

Now by expanding the eigenvectors in the Fourier basis,

$$|\omega_{lk}) = \sum_j \left[\tilde{\mathbf{B}}_{lk}\right]_j |\varphi_j)\ , \tag{108}$$

Eqs. 100 and 101 are rewritten as

$$\tilde{\mathbf{U}}_l \tilde{\mathbf{B}}_{lk} = u_{lk} \tilde{\mathbf{U}}_0 \tilde{\mathbf{B}}_{lk}\ ;\ \ \tilde{\mathbf{B}}_{lk}^{\mathrm{T}} \tilde{\mathbf{U}}_0 \tilde{\mathbf{B}}_{lk} = 1 \tag{109}$$

for $l = 1, ..., \mathrm{D}$. The amplitudes are then obtained from the eigenvectors as

$$\sqrt{d_k} = \tilde{\mathbf{B}}_{lk}^{\mathrm{T}} \tilde{\mathbf{C}} \ , \tag{110}$$

where the coefficients of the $1 \times (K_{\mathrm{win}} + K_{\mathrm{c}})$ column vector $\tilde{\mathbf{C}}$ are computed using the following D-dimensional FT of the original signal array $\mathbf{C}$:

$$\left[\tilde{\mathbf{C}}\right]_j = \sum_{\substack{n_r=0 \\ r=1,\dots,\mathrm{D}}}^{M_{rj}-1} e^{i\vec{n}\vec{\varphi}_j} c_{\vec{n}} \ , \quad j = 1, ..., K_{\mathrm{win}} + K_{\mathrm{c}} \ . \tag{111}$$

Although the numerical bottleneck of the D-dimensional FDM is usually associated with the solution of the generalized eigenvalue problems, Eq. 109, an intelligent programming of these expressions to compute the U-matrices is desirable. For example, the use of globally equidistant grids allows one to evaluate all the D-dimensional Fourier sums using certain fast FT algorithms which have the FFT scaling even when the signal size is not a power of two (e.g., FFTW, the Fastest Fourier Transform in the West [51]), making the overall U-matrix construction for all the windows scale as FFT. An additional saving is possible if one takes advantage of the fact that some of the Fourier sums are related to each other via simple recursion relations (see refs. [12, 11]). Also note, that even unintelligently programmed, Eqs. 105 - 107 will scale as $\sim N_{\mathrm{total}} \times (K_{\mathrm{win}} + K_{\mathrm{c}})$ for a single window, which is still acceptable.

8.4. Why does the naive D> 1 FDM "fail" for noisy data?

Unlike the 1D FDM where a failure would be a rare exclusion from the rule, its naive D-dimensional generalization would typically fail for a general input data, the method being successful only when the signal is strictly of the form of Eq. 90 with high SNR and the local completeness relation (compare with Eq. 69),

$$\rho(\vec{\varphi}_j) \approx \prod_{l=1}^{\mathrm{D}} \frac{N_l \tau_l}{4\pi} \geq \rho(\vec{\omega}_k) \ , \tag{112}$$

satisfied for the density $\rho(\vec{\varphi}_j)$ of the grid points $\vec{\varphi}_j$ and the density $\rho(\vec{\omega}_k)$ of poles $\vec{\omega}_k$.

Firstly, construction of a D-dimensional line list requires uniqueness of the set $\{\tilde{\mathbf{B}}_{1k}\}$, which is not the case for degenerate frequencies. However, the NMR signals often contain degenerate frequencies (the cross peaks) which makes the degenerate case general for NMR.

Secondly, even if the spectrum is not degenerate, the assumption that the eigenvectors $\tilde{\mathbf{B}}_{lk}$ are the same for different values of l is hardly applicable to noisy data. Practically, for low SNR the sets of the eigenvectors corresponding to different l might not even be close to each other. Apparently, there is no easy way to "couple" the frequencies ω_{lk} obtained by solving Eq. 109 with different l. That is, at a time one can only have any particular projection of the line list $\{\omega_{lk}, d_{lk}\}$ with the amplitudes

$$\sqrt{d_{lk}} = \tilde{\mathbf{B}}_{lk}^{\mathrm{T}} \tilde{\mathbf{C}} \ , \tag{113}$$

but not the whole line list $\{\vec{\omega}_k, d_k\}$, as was originally assumed. This, in turn, implies that Eq. 92 is generally not very useful for an accurate spectral estimation as it relies on the existence of a coupled and accurate line list.

Thirdly, it might appear that Eq. 103 can be used to couple the frequencies. However, Eq. 103, albeit theoretically correct, is practically quite useless as it is not variational with respect to the eigenvalues u_{lk}. That is, errors in the eigenvectors $\tilde{\mathbf{B}}_{1k}$ cause unacceptable errors in the eigenvalues u_{lk} estimated by Eq. 103 with $l \neq 1$.

A somewhat complicated procedure of coupling the frequencies in 2D FDM was used in refs [3, 6, 5] with relative success. This procedure, based on diagonalization of more than two different evolution operators, e.g. $\hat{U}_1$, $\hat{U}_2$ and $\hat{U}_{\vec{p}} = \hat{U}_1\hat{U}_2$, would result in three independent line lists with frequencies $\{\omega_{1k}\}$, $\{\omega_{2k}\}$ and $\{\omega_{\vec{p}k}\}$, respectively. Coupling these sets of frequencies into an integrated 2D line list can be carried out by finding such an ordering of frequencies for which $\sum_k |\omega_{1k} + \omega_{2k} - \omega_{\vec{p}k}|$ is minimized. Unfortunately, this method is only reliable for signals with sufficiently high SNR.

In ref. [8] an interesting idea of "simultaneous diagonalization" of all the U-matrices that occur in Eq. 109 was explored for the 2D case. Roughly speaking, the idea is to find a unitary transformation applied simultaneously to all the U-matrices that would minimize the sum of all the off-diagonal elements. As such one can obtain a complete coupled line list by sacrificing the accuracy of the frequencies (eigenvalues) and amplitudes (eigenvectors). The obvious drawback of this method is that instead of using the existing eigen-solver algorithms one has to solve a non-linear optimization problem, i.e., what we have been trying to avoid by using linear algebra.

9. THE RESOLVENT FORMULAE FOR MULTIDIMENSIONAL SPECTRAL ESTIMATION.

The method of spectral estimation presented in this section avoids the problem of constructing the coupled D-dimensional line list. That is, here we are not trying to solve the D-dimensional HIP of Eq. 90. Although we still assume the quantum mechanical ansatz of Eq. 94 to be valid and the Hamiltonians $\hat{\Omega}_l$ to commute, but we let the eigenbases $\{|\omega_{lk})\}$ be l-dependent. This, in particular, covers the case of degenerate spectra, but, most importantly, avoids the necessity of generating a unique eigenbasis.

Just as in the 1D case (see Eq. 38), the spectral function formally defined as a D-dimensional FT of the signal (Eq. 92) can also be written in terms of the resolvent operators,

$$I^\tau(s_1, ..., s_{\mathrm{D}}) = (0|\hat{G}^{\tau_1}(s_1)...\hat{G}^{\tau_{\mathrm{D}}}(s_{\mathrm{D}})|0) \ . \tag{114}$$

Since each $\hat{G}^{\tau_l}(s_l)$ can be represented using Eq. 30, expression (114) is representable by ω_{lk} and $\tilde{\mathbf{B}}_{lk}$, that can, in turn, be obtained by solving the D generalized eigenvalue equations (109), independently for each $l = 1, ..., \mathrm{D}$, because $(\omega_{lk}|\omega_{l'k'}) = \tilde{\mathbf{B}}_{lk}^{\mathrm{T}}\tilde{\mathbf{U}}_0\tilde{\mathbf{B}}_{l'k'}$ and $(0|\omega_{lk}) = \sqrt{d_{lk}} \equiv \tilde{\mathbf{C}}^{\mathrm{T}}\tilde{\mathbf{B}}_{lk}$. For instance, one can use the following expression,

$$\begin{aligned} I^\tau(s_1, ..., s_{\mathrm{D}}) &= \sum_{k_1,...,k_{\mathrm{D}}} \tilde{\mathbf{C}}^{\mathrm{T}}\tilde{\mathbf{B}}_{1k_1}\tilde{\mathbf{B}}_{1k_1}^{\mathrm{T}}\tilde{\mathbf{U}}_0\tilde{\mathbf{B}}_{2k_2}... \\ &\times \ \tilde{\mathbf{B}}_{(\mathrm{D}-1)k_{\mathrm{D}-1}}^{\mathrm{T}}\tilde{\mathbf{U}}_0\tilde{\mathbf{B}}_{\mathrm{D}k_{\mathrm{D}}}\tilde{\mathbf{B}}_{\mathrm{D}k_{\mathrm{D}}}^{\mathrm{T}}\tilde{\mathbf{C}}\prod_{l=1}^{\mathrm{D}} G_{lk_l}^{\tau_l}(s_l) \ . \end{aligned} \tag{115}$$

Eq. 115 can be used instead of the conventional D-dimensional FT to estimate the D-dimensional complex spectrum. A D-dimensional absorption mode spectrum can be defined by modifying Eq. 114 using the spectral density operators (32):

$$A^\tau(s_1, ..., s_{\mathrm{D}}) = (0|\hat{\delta}^{\tau_1}(s_1)...\hat{\delta}^{\tau_{\mathrm{D}}}(s_{\mathrm{D}})|0) \ , \tag{116}$$

which after using the spectral representation becomes

$$\begin{aligned} A^\tau(s_1,...,s_{\rm D}) &= \sum_{k_1,\ldots,k_{\rm D}} \tilde{\mathbf{C}}^{\rm T}\tilde{\mathbf{B}}_{1k_1}\tilde{\mathbf{B}}_{1k_1}^{\rm T}\tilde{\mathbf{U}}_0\tilde{\mathbf{B}}_{2k_2}... \\ &\times\ \tilde{\mathbf{B}}_{({\rm D}-1)k_{{\rm D}-1}}^{\rm T}\tilde{\mathbf{U}}_0\tilde{\mathbf{B}}_{{\rm D}k_{\rm D}}\tilde{\mathbf{B}}_{{\rm D}k_{\rm D}}^{\rm T}\tilde{\mathbf{C}}\prod_{l=1}^{\rm D}\delta_{lk_l}^{\tau_l}(s_l)\ . \end{aligned} \tag{117}$$

Note, that this expression leads to absorption lineshapes no matter whether or not the signal was phased prior to the processing. $A^\tau(s_1,...,s_{\rm D})$ is, in principle, a complex valued function, although in the case of all real amplitudes it becomes purely real. Note that the above spectral representations are not unique as similar expressions can be obtained by permutations of the indices. The absorption mode formula, Eq. 117, is meaningful only if the different peaks with absorption shapes are not overlapping too much, i.e., the interference effects are not significant.

In many cases the full dimensionality spectra are not always desired as they might have too many details, be too difficult to visualize, interpret and store. Various reduced dimensionality spectral projections are often used to simplify the problem of interpreting the data. As a particular example we here give expressions for 2-dimensional standard projections of the D-dimensional spectra (where D≥ 2):

$$\begin{aligned} I^\tau(s_1,s_2) &= \sum_{k_1,k_2}\tilde{\mathbf{C}}^{\rm T}\tilde{\mathbf{B}}_{1k_1}\tilde{\mathbf{B}}_{1k_1}^{\rm T}\tilde{\mathbf{U}}_0\tilde{\mathbf{B}}_{2k_2}\tilde{\mathbf{B}}_{2k_2}^{\rm T}\tilde{\mathbf{C}} \\ &\times\ G_{1k_1}^\tau(s_1)G_{2k_2}^\tau(s_2)\ , \end{aligned} \tag{118}$$

$$\begin{aligned} A^\tau(s_1,s_2) &= \sum_{k_1,k_2}\tilde{\mathbf{C}}^{\rm T}\tilde{\mathbf{B}}_{1k_1}\tilde{\mathbf{B}}_{1k_1}^{\rm T}\tilde{\mathbf{U}}_0\tilde{\mathbf{B}}_{2k_2}\tilde{\mathbf{B}}_{2k_2}^{\rm T}\tilde{\mathbf{C}} \\ &\times\ \delta_{1k_1}^\tau(s_1)\delta_{2k_2}^\tau(s_2)\ . \end{aligned} \tag{119}$$

Note that the expressions in Eqs. 115-119 are not numerically as expensive as they might seem: the multiple summations can be evaluated successively.

9.1. 2D RRT.

Similarly to Eq. 56 it is also worth rewriting the spectral projection in a matrix form that does not necessarily require evaluation of the eigenvectors and eigenvalues of the generalized eigenvalue problems [14], for example,

$$\begin{aligned} I^\tau(s_1,s_2) &= \tilde{\mathbf{C}}^{\rm T}\Big\{\tilde{\mathbf{R}}_{1q}(s_1)^{-1}\tilde{\mathbf{U}}_0\tilde{\mathbf{R}}_{2q}(s_2)^{-1} \\ &-\ \frac{i}{2}\left[\tau_2\tilde{\mathbf{R}}_{1q}(s_1)^{-1}+\tau_1\tilde{\mathbf{R}}_{2q}(s_2)^{-1}\right]\Big\}\tilde{\mathbf{C}}-\frac{\tau_1\tau_2c_0}{4} \end{aligned} \tag{120}$$

with $\tilde{\mathbf{R}}_{ql}(s_l)^{-1}$, $l=1,2$, defining two regularized inverses of the matrices

$$\tilde{\mathbf{R}}_l(s_l)=\frac{\tilde{\mathbf{U}}_0-e^{i\tau_l s_l}\tilde{\mathbf{U}}_l}{i\tau_l}\ ,\quad l=1,2\ . \tag{121}$$

The regularization may now be carried out by either SVD (Eqs. 60, 62) or by Tikhonov regularization (63). With the latter one can proceed by first computing the two frequency-dependent vectors $\tilde{\mathbf{X}}_l(s_l),\ l=1,2$, by solving the two regularized Hermitian least squares problems,

$$\left(\tilde{\mathbf{R}}_l(s_l)^\dagger\tilde{\mathbf{R}}_l(s_l)+q^2\right)\tilde{\mathbf{X}}_l(s_l)=\tilde{\mathbf{R}}_l(s_l)^\dagger\tilde{\mathbf{C}}\ , \tag{122}$$

with regularization parameter q, and then using

$$\begin{aligned} I^\tau(s_1,s_2) &= \tilde{\mathbf{X}}_1(s_1)^{\mathrm{T}}\tilde{\mathbf{U}}_0\tilde{\mathbf{X}}_2(s_2)-\frac{\tau_1\tau_2c_0}{4} \\ &- \frac{i}{2}\tilde{\mathbf{C}}^{\mathrm{T}}\left[\tau_2\tilde{\mathbf{X}}_1(s_1)+\tau_1\tilde{\mathbf{X}}_2(s_2)\right]\ . \end{aligned} \tag{123}$$

Note that the total number of the linear systems to be solved for each 2D frequency window is equal to $N_{s_1}+N_{s_2}$, where N_{s_1} and N_{s_2} are the numbers of the frequency grid points, s_1 and s_2, to plot the spectrum in the window.

Some numerical examples of implementing the 2D RRT can be found in ref. [14].

10. REGULARIZATION OF MULTIDIMENSIONAL FDM.

Our first applications of 2D FDM dealt with signals with relatively high SNR and essentially no dangerous degeneracies that could complicate the line list construction [3, 5, 6]. So the early successes of the "naive" version of the 2D FDM might appear a little bit misleading. The resolvent formulae [9, 10, 12] have made FDM spectra more stable with respect to both noise and degeneracies, but these spectra would generally be unsatisfactory for relatively low SNR signals where the FT could still provide quite high resolution, given the signals of sufficiently large size. An instability in the 1D FDM could occur only for exotic signals and is completely eliminated by the use of multiscale basis. Unlike the 1D case, in the $D>1$ FDM the instability is rather the rule and is difficult to eliminate. A typical example is shown in the upper left panel of Fig. 6 where an absorption 2D HSQC spectrum of progesterone was computed by FDM without any regularization using a purely phase modulated 2D signal. The pulse sequence and other details of this particular NMR experiment can be found in refs. [6, 13]. The spectrum has a high resolution character, however it is contaminated by various artifacts, such as spurious spikes randomly distributed over the frequency domain and poorly converged genuine peaks. Moreover, this artifact patern is very sensitive to both the small variations in the input data and the parameters of the FDM calculation.

At this point it is still not absolutely clear what exactly causes instability in the 2D FDM. One possible explanation is based on the comparison between the 1D and 2D implementations of FDM. In the 1D FDM a signal of size N leads (with the Krylov basis) to a generalized eigenvalue problem of rank $M_{\mathrm{Krylov}}=N/2$, which, in turn, yields $N/2$ pairs of (ω_k,d_k), i.e., totally N parameters. This means that the solution of the HIP, Eq. 11, is unique with the total number of equations exactly matching the total number of unknowns, i.e., in principle, no other regularization constraints are needed. In the 2D case the situation is different. In Krylov basis the total rank of the U-matrices is $M_{\mathrm{Krylov}}=N_1N_2/4$, resulting in $N_1N_2/4$ frequencies ω_{lk} for each generalized eigenvalue problem, Eq. 109. If, according to the form of Eq. 90 with D=2, we assume the total number of 2D Lorentzian peaks (each characterized by two frequencies ω_{1k} and ω_{2k} and an amplitude d_k) to be M_{Krylov}, we will have to deal with an overdetermined problem with totally N_1N_2 equations and $\frac{3}{4}N_1N_2$ unknowns. Therefore, for general fixed size array c_{n_1,n_2} the exact solution of the 2D HIP using the number of parameters consistent with the FDM procedure, strictly speaking, does not exist, however, when solving the 2D HIP by FDM we implicitly assume that the data set can be fit by the parametric form of Eq. 90, i.e., we assume that this data *is not generic.*

The above explanation does not pretend to be absolutely correct but at least it confirms that there is something wrong with the 2D HIP, or, in other words, the 2D HIP is an *incorrectly posed problem*, which requires some *regularization*.

Apparently, an ill-defined linear system, $\mathbf{RX} = \mathbf{C}$, can be regularized in a very straightforward fashion, as discussed in Section 5, by either SVD or Tikhonov regularization. At the same time, there seems to be no obvious extension of such techniques to the case of generalized eigenvalue problems encountered in FDM. As pointed out by Moler and Stewart [44], when the two matrices in the left and right hand sides of Eq. 109 have a common null space (as is the case in FDM), the problem has unusually pathological features. In particular, it was not recommended to apply SVD to $\mathbf{U}_0$ (in order to get rid of the null subspace) for the reason that the eigenvalues and eigenvectors become very sensitive to the assumed rank of the range subspace, introducing an element of arbitrareness. On the other hand, the QZ algorithm developed in ref. [44] was argued to provide accurate eigenvalues and eigenvectors in terms of two numbers, $u_k = \alpha_k/\beta_k$, the accuracy of which is not affected by the ill-conditioned structure of the matrices. It was also argued that the "unreliable" eigenvalues could be identified by smallness of both α_k and β_k. Our experience with 2D FDM is somewhat contradictory to the recommendations of Moler and Stewart as according to the above discussion these accurate eigenvalues and eigenvectors are generally useless, while the truncated SVD of $\mathbf{U}_0$ may help in removing the artifacts, although the ambiguity in deciding how many basis vectors should be retained remains a major problem. For the latter reason the use of the truncated SVD was not extensively exploited in our publications.

10.1. Signal averaging.

The ambiguity in choosing the regularization parameter, especially in the truncated SVD, may appear quite unfriendly. A simple solution to avoid it was suggested in refs. [9, 10]. It takes advantage of the randomness of the artifacts appearing in the spectrum upon changing the signal size when no (or very mild) regularization is implemented. That is, when sufficiently large number of FDM spectra calculated using different N_1 are summed together, these artifacts magically average out. We call this method the *signal size averaging*. It may be applicable in situations where the signal is sufficiently long in at least one dimension, e.g., the running time. Assuming the artifacts in different spectra to be uncorrelated, the averaging will improve the SNR of the FDM ersatz spectrum by a factor of $\sqrt{N_{\mathrm{FDM}}}$. One should though realize that only the artifacts caused by imperfections of FDM are removed by such an averaging, not the actual noise present in the signal. An example of such an averaged spectrum is shown in ref. [13]. Note also, that the spectra in Figs. 7 and 8 were obtained by signal size averaging.

An obvious and major drawback of the method is that $N_{\mathrm{FDM}} \sim 10 - 100$ (rather than one) FDM calculations have to be performed, significantly increasing the overall numerical effort. Another serious drawback is that an averaged spectrum does not correspond to a compact line list. It is the latter reason, though, which explains the averaging phenomenon. Namely, the huge number of parameters from different FDM calculations used to construct the averaged spectrum eliminate the overdeterminicity problem of a single solution of the 2D HIP.

10.2. Pseudo-noise averaging.

Here we describe another way to perform regularization by averaging [12] which could also be very useful in cases when the processing time is not a big issue. Instead of changing the signal length we can exploit the great sensitivity of the output spectrum to small variations of the input signal of fixed size. This sensitivity may be observed by, e.g., comparing FDM spectra $A(s_1, s_2)$ obtained from a 2D signal perturbed by different realizations of a small uniformly distributed noise:

$$c_{\vec{n}} \to c_{\vec{n}} + q y_{\vec{n}} \tag{124}$$

with $\langle y_{\vec{n}} \rangle = 0$, $\langle |y_{\vec{n}}|^2 \rangle = 1$ and q, the level of the pseudo-noise.

Most surprizingtly, if q is sufficiently large, an artifact free spectrum may be obtained by Monte Carlo averaging of $A^{\tau}(s_1, s_2)$ over sufficiently many differnt realizations of $y_{\vec{n}}$.

Note, that the signal size averaging has essentially no free parameter and is limited by the maximum signal size (i.e., $N_{\rm FDM}$ is limited), while the pseudo-noise averaging converges similarly with respect to the number of samples $N_{\rm FDM}$, but $N_{\rm FDM}$ can be arbitrary. The fact that the pseudo-noise amplitude q can be varied may be considered as both an advantage (since the result as a function of q can be very useful) and a disadvantage (since one has to figure out an optimal q).

Interestingly, the pseudo-noise averaging can also be implemented at the stage of solving Eq. 109 by adding pseudo-noise to the U-matrices computed from the original unperturbed signal. The qualitative explanation is that the U-matrices are linear functionals of the input signal $c_{\vec{n}}$ and, therefore, a variation in the signal $y_{\vec{n}}$ transfers linearly into the variation of the U-matrices:

$$\tilde{\mathbf{U}}_l \to \tilde{\mathbf{U}}_l + q\tilde{\mathbf{Y}} \ , \tag{125}$$

where $\tilde{\mathbf{Y}}$ is a complex symmetric matrix with independent random coefficients satisfying $\langle [\tilde{\mathbf{Y}}]_{jj'} \rangle = 0$, $\langle |[\tilde{\mathbf{Y}}]_{jj'}|^2 \rangle = 1$.

To this end, we describe the simplest implementation of the pseudo-noise averaging to obtain a 2D double-absorption spectral projection from a purely phase modulated signal. We first rewrite Eq. 119 in the form

$$A^{\tau}(s_1, s_2) = \tilde{\mathbf{X}}_{1q}(s_1)^{\rm T} \tilde{\mathbf{U}}_0 \tilde{\mathbf{X}}_{2q}(s_2) \ , \tag{126}$$

where the absorption-mode vectors $\tilde{\mathbf{X}}_{lq}(s_l)$ are computed independently for each $l = 1, 2$ using the eigenfrequencies and eigenvectors of the corresponding perturbed generalized eigenvalue problems,

$$\left(\tilde{\mathbf{U}}_l + q\tilde{\mathbf{Y}}\right) \tilde{\mathbf{B}}_{lk} = u_{lk} \tilde{\mathbf{U}}_0 \tilde{\mathbf{B}}_{lk} \ , \tag{127}$$

and then averaged over a sufficient number, $N_{\rm FDM}$, of realizations of the random perturbation $\tilde{\mathbf{Y}}$ as

$$\tilde{\mathbf{X}}_{lq}(s_l) = \left\langle \sum_k \delta^{\tau_l}_{lk}(s_l) \tilde{\mathbf{B}}_{lk} \tilde{\mathbf{B}}^{\rm T}_{lk} \tilde{\mathbf{C}} \right\rangle_{\tilde{\mathbf{Y}}} \tag{128}$$

Obviously, q here plays the role of a regularization parameter. We found that the behaviour of the spectra regularized by the pseudo-noise averaging as a function of q for the signal processed in Fig. 6 to be very similar to that displayed in the figure. However, we believe that the pseudo-noise averaging is a much more general regularization procedure, than that implemented in Fig. 6, and may be used in many different contexts with, yet, the two serious drawbacks, the high computational cost and inability to construct a line list. Therefore, when these aspects are crucial, one wants to implement a regularization in the spirit of the truncated SVD.

10.3. Optimistic regularization: FDM2k.

A rather more attractive method than the truncated SVD seems to be the procedure, reminiscent to the Tikhonov regularization, in which Eq. 109 for each $l = 1, ..., \mathrm{D}$ is modified as [15]

$$\tilde{\mathbf{U}}_0^\dagger \tilde{\mathbf{U}}_l \tilde{\mathbf{B}}_{lk} = u_{lk} \left(\tilde{\mathbf{U}}_0^\dagger \tilde{\mathbf{U}}_0 + q^2 \right) \tilde{\mathbf{B}}_{lk} \ , \tag{129}$$

with regularization parameter q. The new generalized eigenvalue equations have a Hermitian and positive definite right hand side matrix, which may be advantageous for numerical solution. It is very tempting to treat q as the "noise power", just like in the Maximum Entropy applications [43]. Indeed, it can be demonstrated semiquantitatively [15], that the spectral features with amplitudes d_k of order of q and below are smoothed out, while the stronger peaks remain essentially unaffected. However, how the spectra are distorted (regularized) by q is still not fully understood. Quite surprisingly, the results of using Eq. 129 for some 2D [15] applications are very encouraging, although the element of ambiguity in the choice of q is still the main issue. It is, therefore, recommended to generate a family of spectra as a function of q, treating the latter as a parameter of the method, just like the form of apodization function in DFT.

The regularization corresponding to the use of Eq. 129 has been tested for some 2D HSQC spectra and showed good results. It had been named *FDM2k* [15] to honor the new Millennium. FDM2k is demonstrated in Fig. 6. The spectra change very smoothly with the regularization parameter q, when the latter varies by an order of magnitude. A small q gives highly resolved multiplets but also retains some small spikes. When q is increased the spectrum becomes more uniform and smooth with decreasing resolution. With large values of q the multiplet structure is unresolved and some generally weak peaks disappear in the contourplot as they are effectively broadened by the regularization. Note that the spectrum corresponding to $q = 0.01$ is much better resolved than that in ref. [6] where a "naive" 2D FDM was used. Also note that in ref. [6] the signal was much shorter in the running time dimension to simplify the frequency identification procedure, which is completely avoided here due to the use of the resolvent formulae.

10.4. Pessimistic and complicated regularization to compute double-absorption spectra.

FDM2k allows one to compute a double-absorption spectrum from a purely phase modulated signal using a simple and inexpensive trick, Eq. 129. Note, however, that the regularization of $\mathbf{U}_0$ does not completely remove the singularities of $\tilde{\mathbf{R}}(s_l)$, which can still have some accidental degeneracies leading to artifacts in the spectrum. Therefore, most consistent, but pessimistic, approach is to regularize $\tilde{\mathbf{R}}(s_l)$ itself for every frequency s_l, as in RRT. However, the 2D RRT expressions, presented above, allow one to estimate only a complex infinite-time 2D DFT, while calculating a double-absorption spectrum by 2D RRT is not as straightforward as using 2D FDM. The reason is that the convenient structure of a matrix pencil, $\tilde{\mathbf{U}}_0 - z\tilde{\mathbf{U}}_l$, (which has a spectral representation in terms of the eigenvalues and eigenvectors of the corresponding generalized eigenvalue problem) is destroyed in the regularized resolvent. Here we demonstrate how this difficulty can be circumvented using the definition of the imaginary part of an operator (31), albeit significantly increasing the numerical effort. For example, a 2D double-absorption RRT could be written as

$$A^\tau(s_1, s_2) = \tilde{\mathbf{C}}^{\mathrm{T}} \tilde{\boldsymbol{\delta}}_1(s_1) \tilde{\mathbf{U}}_0 \tilde{\boldsymbol{\delta}}_2(s_2) \tilde{\mathbf{C}} \ , \tag{130}$$

where the matrices

$$\tilde{\boldsymbol{\delta}}_l(s_l) = \sum_k \mathrm{Im} \left\{ \frac{1}{r_{lk}} - \frac{i\tau}{2} \right\} \tilde{\mathbf{B}}_{lk} \tilde{\mathbf{B}}_{lk}^{\mathrm{T}} \ , \quad l = 1, 2, \tag{131}$$

have originated from the spectral density operators $\hat{\delta}^{\tau_l}(s_l)$ and can be evaluated by solving (in the worst scenario, at each frequency s_l) the following generalized eigenvalue problems,

$$\tilde{\mathbf{R}}_{lq}(s_l)\tilde{\mathbf{B}}_{lk} = r_{lk}\tilde{\mathbf{U}}_{0q}\tilde{\mathbf{B}}_{lk} \ ; \ \ \tilde{\mathbf{B}}_{lk}^{\mathrm{T}}\tilde{\mathbf{U}}_{0q}\tilde{\mathbf{B}}_{lk} = 1 \ , \tag{132}$$

where, as before, the additional subscript q stands for regularized matrices.

Eqs. 130-132 are new. Their efficient numerical implementation is not obvious as one seems to have to compute an expensive SVD of $\tilde{\mathbf{R}}_l(s_l)$ for different values of the frequency argument s_l and then solve the corresponding eigenvalue problems (132) with the regularized matrices $\tilde{\mathbf{R}}_{lq}(s_l)$ and $\tilde{\mathbf{U}}_{0q}$.

Since $\tilde{\mathbf{R}}_{lq}(s_l)$ is a function of s_l, in principle, both r_{lk} and $\tilde{\mathbf{B}}_{lk}$ are functions of s_l. However, approximately, $\tilde{\mathbf{B}}_{lk}$ is a very smooth function of s_l, while r_{lk} can be parametrized as

$$r_{lk} \approx \frac{1 - e^{i\tau_l(s_l - \omega_{lk})}}{i\tau_l} \tag{133}$$

with ω_{lk}, a smooth function of s_l. This circumstance can be utilized to reduce the computational burden, which will be explored in our future publications.

11. 45$^{\mathrm{O}}$ PROJECTIONS IN 2D, 3D AND 4D EXPERIMENTS: *SINGLET*-PROTON, *SINGLET*-HSQC AND *SINGLET*-TOCSY SPECTRA.

Besides the trivial projections, such as that in Eq. 119, obtained by integrating out and 117 some of the frequency dependencies in Eqs. 115, one can consider non-trivial projections. Examples of the latter include the 45^o projections in the 2D-J experiments [9, 10] and their 3D and 4D analogs [12, 13]. Another interesting projection was considered in ref. [16] where the 2D DOSY spectra were plotted as a function of the conventional proton and non-conventional "diffusion" dimension formally corresponding to the imaginary frequency argument.

Let $\vec{p} = (p_1\tau_1, ..., p_{\mathrm{D}}\tau_{\mathrm{D}})$ be a general vector in the D-dimensional time space along which we seek to construct a spectral projection. In principle, p_l could be complex numbers (as in ref. [16]). The $\vec{p}$-projections of the frequencies could be defined as

$$\omega_{\vec{p}k} = \frac{\vec{p}\vec{\omega}_k}{\tau_1} \equiv \sum_{l=1}^{\mathrm{D}} \frac{p_l\tau_l}{\tau_1}\omega_{lk} \ . \tag{134}$$

The normalization term $\frac{1}{\tau_1}$ is arbitrary and not essential since it only changes the scale. We can now define the complex and absorption-mode spectral $\vec{p}$-projections as

$$I_{\vec{p}}(s) \ = \ \sum_k d_k G_{\vec{p}k}(s) \ , \tag{135}$$

$$A_{\vec{p}}(s) \ = \ \mathrm{Im}\left\{I_{\vec{p}}(s)\right\} \ , \tag{136}$$

where we used the integral Fourier spectral representation rather than the discrete one as the latter would unlikely be advantageous for a non-trivial projection. We also used the simplest expression to evaluate the 1D absorption spectrum that assumes all amplitudes to be real.

Rather than constructing the projected line list out of the complete D-dimensional one, a much less demanding approach is by following ref. [12] where the frequency $\vec{p}$-projections are defined as the eigenvalues of the projected Hamiltonian

$$\hat{\Omega}_{\vec{p}} = \frac{\vec{p}\vec{\Omega}}{\tau_1} \equiv \sum_{l=1}^{\mathrm{D}} \frac{p_l \tau_l}{\tau_1} \hat{\Omega}_l \tag{137}$$

and

$$\hat{\Omega}_{\vec{p}} |\omega_{\vec{p}k}) = \omega_{\vec{p}k} |\omega_{\vec{p}k}) \ , \tag{138}$$

where as before the eigenfunctions $|\omega_{\vec{p}k})$ of $\hat{\Omega}_{\vec{p}}$ depend on $\vec{p}$ (because of either degeneracies or noise or both), although we still assume that $\hat{\Omega}_{\vec{p}}$ commutes with $\hat{\Omega}_l$ for any l. The corresponding resolvent expression for the spectral $\vec{p}$-projection is

$$I_{\vec{p}}(s) = (0|\hat{G}_{\vec{p}}(s)|0) \ . \tag{139}$$

To this end the 45^o projection of a 2D-J spectrum corresponds to $\vec{p} = (\tau_1, -\tau_1)$, in which the proton multiplets collapse to single peaks at the frequencies of the proton chemical shifts. In the FFT framework construction of absorption-mode 45^o projections is impossible, so only a skew 45^o projection of an absolute value 2D-J spectrum [39] can be used.

The procedure of calculating the $\vec{p}$-projections developed in ref. [9] for the 2D-J experiment is generalized in ref. [12] to the case of arbitrary $\vec{p}$ and D.

Given matrix representations $\tilde{\mathbf{U}}_l$ for $l = 0, ..., \mathrm{D}$ in a Fourier window basis $|\varphi_j)$, Eqs. 105-107, a numerical procedure of calculating a $\vec{p}$-projection can be based on the following steps.
(i) Solve independently D generalized eigenvalue problems (109) to obtain the eigenvalues $u_{lk} \equiv e^{-i\tau_l \omega_{lk}}$ and eigenvectors $\tilde{\mathbf{B}}_{lk}$.
(ii) Use ω_{lk} and $\tilde{\mathbf{B}}_{lk}$ to construct a matrix representation of $\hat{\Omega}_{\vec{p}}$ in the basis of $|\varphi_j)$,

$$\tilde{\mathbf{\Omega}}_{\vec{p}} = \sum_{l=1}^{\mathrm{D}} \frac{p_l \tau_l}{\tau_1} \tilde{\mathbf{\Omega}}_l = \sum_{l=1}^{\mathrm{D}} \frac{p_l \tau_l}{\tau_1} \sum_k \omega_{lk} \tilde{\mathbf{U}}_0 \tilde{\mathbf{B}}_{lk} \tilde{\mathbf{B}}_{lk}^{\mathrm{T}} \tilde{\mathbf{U}}_0, \tag{140}$$

where $\tilde{\mathbf{\Omega}}_l$ are the corresponding matrix representations of $\hat{\Omega}_l$ in the Fourier window basis.
(iii) Solve another generalized eigenvalue problem

$$\tilde{\mathbf{\Omega}}_{\vec{p}} \tilde{\mathbf{B}}_{\vec{p}k} = \omega_{\vec{p}k} \tilde{\mathbf{U}}_0 \tilde{\mathbf{B}}_{\vec{p}k} \ ; \quad \tilde{\mathbf{B}}_{\vec{p}k}^{\mathrm{T}} \tilde{\mathbf{U}}_0 \tilde{\mathbf{B}}_{\vec{p}k} = 1 \ . \tag{141}$$

(iv) The frequencies $\omega_{\vec{p}k}$ and the amplitudes $d_{\vec{p}k}$, computed from the eigenvectors $\tilde{\mathbf{B}}_{\vec{p}k}$ by Eq. 110, are then used in Eq. 135 (with d_k replaced by $d_{\vec{p}k}$) to compute $I_{\vec{p}}(s)$.

Note, that the fact that there may be many degenerate frequencies among $\omega_{\vec{p}k}$ corresponding, for instance, to the collapsed multiplets in the 45^o projection of a 2D-J spectrum. This though does not make either $I_{\vec{p}}(s)$ or $A_{\vec{p}}(s)$ non-unique. Generally, if there are several degenerate eigenvalues $\omega_{\vec{p}k}$ corresponding to a particular collapsed multiplet, the individual eigenvectors $\tilde{\mathbf{B}}_{\vec{p}k}$ are not well-defined. However, the whole degenerate subspace of these eigenvectors, here called the *single-multiplet subspace*, is unique, subject to an orthogonal complex symmetric transformation within this subspace. This is sufficient for the correct spectral reconstruction using Eq. 135 because the sum of amplitudes $\sum_k d_{\vec{p}k}$ over the single-multiplet subspace should be invariant under any orthogonal transformation of the eigenvectors $\tilde{\mathbf{B}}_{\vec{p}k}$ within the subspace.

Even though the eigenvectors within a degenerate single-multiplet subspace are not defined they can be used to uncover the multiplet cross section [9], e.g., along the acquisition time dimension t_1, by solving the corresponding eigenvalue problem, Eq. 109, with the matrices $\tilde{\mathbf{U}}_1$ and $\tilde{\mathbf{U}}_0$ evaluated in the reduced basis of the single-multiplet subspace. The resulting eigenvalues $u_{1k} = e^{-i\tau_1\omega_{1k}}$ then all belong to this multiplet while the eigenvectors $\tilde{\mathbf{B}}_{1k}$ according to Eq. 110 define the individual amplitudes d_{1k}. These can be used to construct the multiplet cross section.

Because multidimensional FDM works with the entire $N_{\rm total} = N_1 \times N_2 \times \ldots \times N_{\rm D}$ data set, useful projections can be obtained in which a very short additional time dimension is used to simplify a lower-dimensionality spectrum. In Fig. 7 we reproduce an example of a 45^o projection together with the multiplet cross sections of a 2D-J spectrum for ditryptophan tripeptide [9]. The spectra were obtained using just 4 time increments along the J-dimension and were averaged over several FDM calculations with slightly different number of points along the running time dimension. (see Section 10.1 describing FDM regularization by signal averaging.) Note the three overlapping multiplets at ~7.1 ppm and two, at ~7.4 ppm, which are successfully decoupled by this technique.

The idea of proton decoupling by taking a 45^o projection of a 2D-J spectrum to simplify the 1D proton spectrum is quite general and could be very useful to simplify other than 1D proton spectra [12, 13]. For example, proton-carbon HSQC spectrum can be condensed to a *singlet*-HSQC spectrum, in which each CH pair gives rise to a sharp singlet, by a 45^o projection of a 3D HSQC-J spectrum. This particular experiment makes no sense in the context of FT processing because (i) a large number of increments (e.g. 32-64) in the J dimension would be required to achieve a sufficiently high resolution, leading to an unacceptably long experiment time; and (ii) the phase-sensitive 45^o projection vanishes while the absolute-value projection significantly degrades the resolution. As such, each "singlet" in the FT spectrum can give contours as wide as the original multiplet that gave rise to it. By contrast, a useful *singlet*-HSQC spectrum can be obtained using only <u>two</u> time points in the J dimension when FDM is employed [13]. Very narrow absorption-mode resonances are obtained, increasing the resolution substantially. As it is unnecessary to record both N- and P-type spectra, the *singlet*-HSQC spectrum can in fact be obtained in the same total time as a conventional phase-sensitive HSQC spectrum (using FT processing).

An absorption mode *singlet*-HSQC spectrum can be expressed in terms of the spectral density operators as

$$A(s, s_2) = (0|\hat{\delta}_{\vec{p}}(s)\hat{\delta}_2(s_2)|0) \tag{142}$$

where the subscript $\vec{p} \equiv (\tau_1, 0, -\tau_1)$ stands for the 45^o projection in the 2D-J plane with $\hat{\Omega}_{\vec{p}} = \hat{\Omega}_1 - \hat{\Omega}_3$, while "2" corresponds to the projection along the carbon-13 chemical shift dimension. Implementation of these equations is straightforward and is described explicitly in refs. [12, 13] together with several examples. One of those is reproduced in Fig. 8. This spectrum is a $3-1$D simplification of HSQC spectrum of progesterone shown in Fig. 6.

Analogous ideas apply to a double projection of a 4D spectrum resulting in a simplified 2D spectrum. For example as shown in ref. [13] a *singlet*-TOCSY spectrum, in which the 2D multiplets are decoupled, collapsing to singlets, can be obtained by recording two additional data sets with a single J increment in one of the two dimensions and then using a double 45^o projection.

12. REMAINING PROBLEMS.

Both 1D FDM and RRT (that emerged from FDM) are essentially developed and well tested techniques that are generally as reliable as FFT, sufficiently fast, and can often deliver resolution beyond the FT uncertainty relation if the data can be well represented by Lorentzians and is not very noisy.

FDM provides one with an effective evolution operator $\hat{U}$ whose eigenvalues and eigenvectors are directly related to the spectral parameters. However, the difficulties associated with the construction of a meaningful line list for data of poor quality (i.e., not characterized by Eq. 11) exist. These difficulties are not associated with the lack of a reliable algorithm of selecting the "genuine" poles and throwing away the "noise" poles from the full list of complex eigenvalues of $\hat{\Omega}$, but are rather conceptual caused by the ambiguity of the line list for a general data set that, *a priori*, does not fit any particular parametric form.

The multidimensional spectrum cannot be generally constructed from the multidimensional line list as the latter is very hard to obtain. Fortunately, various spectra can be obtained by avoiding the line list construction and using the resolvent expressions. The resolvent operator formalism appears to be very convenient since it allows to construct various types of spectra including absorption-mode spectra, non-trivial spectral projections (e.g., 45^o projections of 2D-J spectra, or 2D singlet-HSQC and singlet-TOCSY spectra, or imaginary frequency projections used in DOSY). The main computational problem associated with the implementation of the resolvent formulae is that one typically deals with very ill-conditioned matrices causing the spectrum to be very unstable with respect to both the FDM parameters and small variations of the input data. Thus, unlike the 1D case, there are major problems to be solved in the multidimensional versions of both FDM and RRT. For instance, for a typical 2D NMR data set, even with relatively high SNR, one has difficulties in constructing two adequate commuting effective evolution operators $\hat{U}_1$ and $\hat{U}_2$ describing the 2D signal. This, in turn, makes it difficult to construct an adequate 2D line list corresponding to Eq. 4. We believe that this problem is, as in the 1D case, a consequence of the ill-defined nature of Eq. 4, although the additional requirement that $\hat{U}_1$ and $\hat{U}_2$ commute makes the problem much worse than in 1D. Clearly, the key issue of D$>$ 1 FDM is to find a general computationally inexpensive and robust procedure that could be applied to regularize the FDM equations. At the present stage the problem is solved only partially. For example, it is possible to regularize RRT which has the high resolution capability of FDM. Unfortunately, RRT can be used only as a spectral estimator and cannot easily overcome some of the DFT limitations. Regularization of RRT is not directly extendable to FDM, although several methods have already been developed, such as truncated SVD of $\mathbf{U}_0$ or FDM averaging. Unfortunately, the former is not generic, while the latter is computationally very expensive and cannot be used to construct a multidimensional line list. The most promising regularization technique, at least for the 2D FDM, is that based on the Tikhonov regularization of $\mathbf{U}_0$ and named FDM2k [15]. Its implementation is computationally very simple and inexpensive, although at this stage it is not clear how general and reliable it is for types of NMR data different from those in ref. [15] and Fig. 6.

To conclude, the main avenues for the future research seem to be the following.

(i) Given the matrix representations of the evolution operators, $\hat{U}_1$,$\hat{U}_2$, etc, in a non-orthonormal basis, to find a fast and reliable method of evaluating various resolvents associated with these operators.

(ii) Given the matrix representations of the evolution operators, to construct a set of commuting effective Hamiltonians $\hat{\Omega}_1$,$\hat{\Omega}_2$, etc., whose eigenvalues and eigenvectors yield the line list.

Both goals are associated with finding a reliable and computationally inexpensive regularization.

ACKNOWLEDGEMENTS.

Some results reviewed in this manuscript were obtained in various collaborative works with Howard Taylor, A.J. Shaka, Jianhan Chen, Joseph Curtis, Geoff Armstrong, Anna De Angelis, Haitao Hu, Que Van, Nathan Taylor and Mari Smith. The author was supported by NSF grant CHE-9807229, and UC BioSTAR grant S97-18. I am particularly grateful to A.J. Shaka and Jianhan Chen for many useful discussions and critical reading of the manuscript. In addition, Jianhan Chen is acknowledged for making some of the figures.

REFERENCES

1. M. R. Wall and D. Neuhauser, Extraction, through filter-diagonalization, of general quantum eigenvalues or classical normal mode frequencies from a small number of residues or a short-time segment of a signal. I. Theory and application to a quantum-dynamics model, *J. Chem. Phys.* **102**, 8011-8022 (1995).

2. V. A. Mandelshtam, and H. S. Taylor, Harmonic inversion of time signals and its applications, *J. Chem. Phys.* **107**, 6756-6769 (1997).

3. V. A. Mandelshtam, and H. S. Taylor, Multidimensional harmonic inversion by filter-diagonalization, *J. Chem. Phys.* **108**, 9970-9977 (1998).

4. J.W. Pang, T. Dieckmann, J. Feigon, D. Neuhauser, Extraction of spectral information from a short-time signal using filter-diagonalization: Recent developments and applications to semiclassical reaction dynamics and nuclear magnetic resonance signals, *J. Chem. Phys.* **108**, 8360-8368 (1998).

5. V. A. Mandelshtam, H. S. Taylor, and A.J. Shaka, Application of the filter diagonalization method to one- and two-dimensional NMR spectra. *J. Magn. Reson.* **133**, 304-312 (1998).

6. V. A. Mandelshtam, H. Hu and A.J. Shaka, Two-dimensional HSQC NMR spectra obtained using a self-compensating double pulsed field gradient and processed using the filter-diagonalization method, *Magn. Res. Chem.* **36**, S17-S28 (1998).

7. H. Hu, Q.N. Van, V. A. Mandelshtam and A.J. Shaka, Reference deconvolution, phase correction and line listing of NMR spectra by the 1D filter diagonalization method. *J. Magn. Reson.* **134**, 76-87 (1998).

8. M.R. Wall, T. Dieckmann, J. Feigon, D. Neuhauser, Two-dimensional filter-diagonalization: spectral inversion of 2D NMR time-correlation signals including degeneracies, *Chem. Phys. Lett.* **291**, 465-470 (1998).

9. V. A. Mandelshtam, Q.N. Van and A.J. Shaka, Obtaining proton chemical shifts and multiplets from several 1D NMR signals, *J. Am. Chem. Soc.* **120**, 12161-2 (1998).

10. V. A. Mandelshtam, N.D. Taylor, H. Hu, M. Smith, and A.J. Shaka, Highly resolved double absorption 2D NMR spectra from complex severely truncated 2D phase modulated signals by filter-diagonalization-averaging method. *Chem. Phys. Lett.* **305**, 209-216 (1999).

11. J. Chen and V. A. Mandelshtam, Multiscale filter diagonalization method for spectral analysis of noisy data with nonlocalized features, *J. Chem. Phys.* **112**, 4429-4437 (2000).

12. V. A. Mandelshtam, The multidimensional filter diagonalization method. I. Theory and numerical implementation, *J. Magn. Reson.* **144**, 343-356 (2000).

13. A. A. De Angelis, H. Hu, V. A. Mandelshtam, and A.J. Shaka, The multidimensional filter diagonalization method. II. Applications to 2D, 3D and 4D NMR experiments, *J. Magn. Reson.* **144**, 357-366 (2000).

14. J. Chen, A.J. Shaka and V. A. Mandelshtam, RRT: The Regularized Resolvent Transform for high resolution spectral estimation, *J. Magn. Reson.* 0000, 0000, (2000).

15. J. Chen, V. A. Mandelshtam and A.J. Shaka, Regularization of the filter diagonalization method: FDM2k, *J. Magn. Reson.* 0000, 0000, (2000).

16. N.M. Loening, J. Keeler, J.E. Curtis, V.A. Mandelshtam and A.J. Shaka, Diffusion ordered spectra obtained using the filter diagonalization method, to be submitted to *J. Magn. Reson.*

17. D. Neuhauser, Bound state eigenfunctions from wave packets - time-energy resolution, *J. Chem. Phys.* **93**, 2611-2616 (1990).

18. V.A. Mandelshtam, T.P. Grozdanov, and H.S. Taylor, Bound states and resonances of the hydroperoxyl radical HO_2. An accurate quantum mechanical calculation using filter diagonalization. *J. Chem. Phys.* **103**, 10074-84 (1995).

19. J.W. Pang, D. Neuhauser, Application of generalized filter-diagonalization to extract instantaneous normal modes. *Chem. Phys. Lett.* **252**, 173-180 (1996).

20. V. A. Mandelshtam, and H. S. Taylor, A low-storage filter diagonalization method for quantum eigenenergy calculation or for spectral analysis of time signals, *J. Chem. Phys.* **106**, 5085-5090 (1997).

21. J. Main, V. A. Mandelshtam, and H. S. Taylor, High resolution recurrence spectra: Beyond the uncertainty principle, *Phys. Rev. Lett.* **78**, 4351-54 (1997).

22. J. Main, V. A. Mandelshtam, and H. S. Taylor, Periodic orbit quantization by harmonic inversion, *Phys. Rev. Lett.* **79**, 825-828, (1997).

23. E. Narevicius, D. Neuhauser, H.J. Korsch, N. Moiseyev, Resonances from short time complex-scaled cross-correlation probability amplitudes by the filter-diagonalization method, *Chem. Phys. Lett.* **276**, 250-4 (1997).

24. R. Chen and H. Guo, Calculation of matrix elements in filter diagonalization: a generalized method based on Fourier transform. *Chem. Phys. Lett.* **279**, 252-8 (1997).

25. F. Grossmann, V. A. Mandelshtam, H. S. Taylor, and J.S. Briggs, Harmonic inversion of semiclassical short time signals, *Chem. Phys. Lett.* **279**, 355-360 (1997).

26. V. A. Mandelshtam, Harmonic inversion of time cross-correlation functions. The optimal way to perform quantum or semiclassical dynamics calculations, *J. Chem. Phys.* **108**, 9999-10007 (1998).

27. V. A. Mandelshtam and M. Ovchinnikov, Extraction of tunneling splittings from a real-time semiclassical propagation. *J. Chem. Phys.* **108**, 9206-09 (1998).

28. G. Jeschke, V.A. Mandelshtam and A.J. Shaka, Pure absorption electron spin echo envelope modulation spectra by using the filter-diagonalization method for harmonic inversion, *J. Magn. Res.* **137**, 221-230 (1998).

29. M.H. Beck and H.-D. Meyer, Extracting accurate bound-state spectra from approximate wave packet propagation using the filter-diagonalization method, *J. Chem. Phys.* **109** 3730-41 (1998).

30. R. Chen and H. Guo, Symmetry-enhanced spectral analysis via the spectral method and filter diagonalization, *Phys. Rev. E* **57** 7288-93 (1998).

31. A.J.R. Da Silva, J.W. Pang, E.A. Carter, D. Neuhauser, Anharmonic vibrations via filter diagonalization of ab initio dynamics trajectories, *J. Phys. Chem. A* **102**, 881-5 (1998).

32. Baron Gaspard Riche de Prony, Essai éxperimental et analytique: sur les lois de la dilatabilité de fluides élastique et sur celles de la force expansive de la vapeur de l'alkool, á différentes températures. Journal de l'École Polytechnique, volume 1, cahier 22, 24-76 (1795).

33. R. de Beer, D. van Ormondt, W.W.F. Pijnappel, Maximum likelihood estimation of poles, amplitudes and phases from 2D NMR time domain signals. (1989 International Conference on Acoustics, Speech and Signal Processing, Glasgow, UK, May 1989) New York, NY, USA: IEEE, 1989. p.1504-7 vol.3.

34. G. Zhu and A. Bax, Two-dimensional linear prediction for signals truncated in both dimensions, *J. Magn. Reson.* **98**, 192-199 (1992).

35. H. Gesmar and J.J. Led, Two-dimensional linear prediction NMR spectroscopy, *J. Magn. Reson.* **83**, 53-64 (1989).

36. H. Gesmar and J.J. Led, The application of the linear prediction principle to NMR spectroscopy, in "Computational aspects of the study of biological macromolecules by nuclear magnetic resonance spectroscopy", (Eds. J.C. Hoch, F.M. Poulson and C. Redfield), pp. 67-85, Plenum Press, New York (1991).

37. G. Bodenhausen, R. Freeman, R. Niedermeyer, and D.L. Turner, Double Fourier transformation in high-resolution NMR, *J. Magn. Reson.* **26**, 133-164 (1977).

38. D.J. States, R.A. Haberkorn and D.J. Ruben, A two-dimensional nuclear Overhauser experiment with pure absorption phase in four quadrants, *J. Magn. Reson.* **48**, 286 (1982).

39. W.P. Aue, J. Karhan, and R.R. Ernst, Homonuclear broad band decoupling and two-dimensional J-resolved NMR spectroscopy, *J. Chem. Phys.* **64**, 4226-4227 (1976).

40. A. Bax, R. Freeman, G.A. Morris, A simple method for suppressing dispersion-mode contributions in NMR spectra - The pseudo echo, *J. Magn. Reson.* **43**, 333-338 (1981).

41. A. Tikhonov, Solution of incorrectly formulated problems and the regularization method, *Soviet Math. Dokl.* **4**, 1035-1038 (1963); A. Tikhonov and V. Arsenin, Solutions of ill-posed problems. Winston and Sons, Washington (1977).

42. S. Sibisi, Two-dimensional reconstructions from one-dimensional data by Maximum-Entropy, *Nature*, 134-136 (1983).

43. J.C. Hoch and A.S. Stern, NMR Data Processing, Wiley-Liss, New York (1996).

44. C.B. Moler and G.W. Stewart, An algorithm for generalized matrix eigenvalue problems, SIAM *J. Numer. Anal.* **10**, 241-256 (1973).

45. A. Neumaier, Solving ill-conditioned and singular linear systems: A tutorial on regularization, WWW:http://solon.cma.univie.ac.at/~neum/

46. S.D. Silverstein and M.D. Zoltowski, The mathematical basis for element and Fourier beamspace MUSIC and root-MUSIC algorithms, *Digital Signal Process.* **1**, 161-175 (1991).

47. J. Tang and J. Norris, LP-ZOOM, a linear prediction method for local spectral analysis of NMR signals, *J. Magn. Reson.* **79**, 190-196 (1988).

48. Y.-Y. Lin; P. Hodgkinson, M. Ernst, A. Pines, A novel detection-estimation scheme for noisy NMR signals: applications to delayed acquisition data. *J. Magn. Reson.* **128**, 30-41 (1997).

49. J. Chen and V.A. Mandelshtam, unpublished results.

50. G.A. Morris, Compensation of instrumental imperfections by deconvolution using an internal reference signal. *J. Magn. Reson.* **80** 547-552 (1988).

51. M. Frigo and S. G. Johnson, FFTW: An Adaptive Software Architecture for the FFT, Proc. ICASSP 1998, vol. 3, p. 1381.

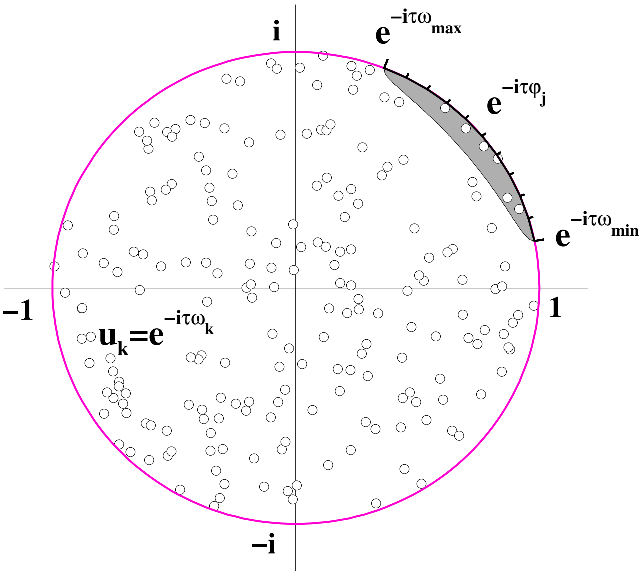

FIG. 1. Schematic plot in the "z-plane" of the eigenvalues $u_k = e^{-i\tau\omega_k}$ of the evolution operator $\hat{U} = e^{-i\tau\hat{\Omega}}$ for the case of strictly decaying signal. Only a small portion (in the shadowed region) of the eigenvalues u_k are extracted by FDM using the grid φ_j in the small frequency interval $[\omega_{\min}, \omega_{\max}]$.

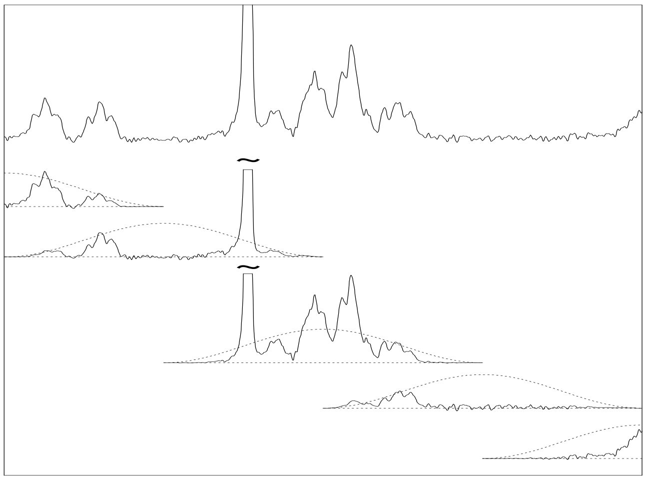

FIG. 2. Decomposition of the spectrum (upper trace) into the overlapping windows using the cosine-weighting functions (Eq. 78) shown with dotted lines.

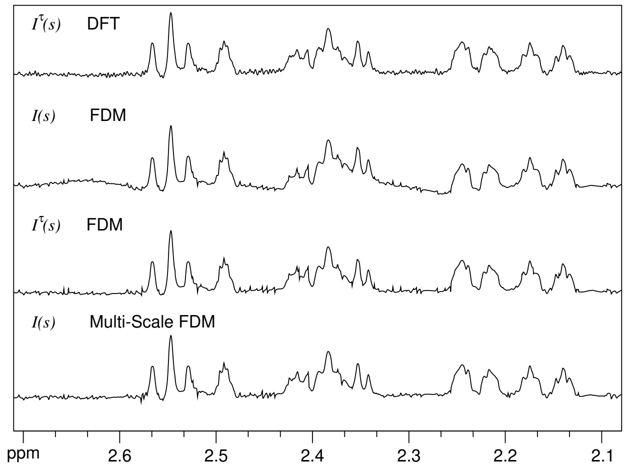

FIG. 3. 1D proton NMR absorption spectrum of progesterone for a representative spectral region of a noisy signal of length $N = 2000$ and spectral width $SW = 4$ ppm (2kHz) computed by, respectively, from the top to the bottom,

- DFT.
- Eq. 13 with spectral parameters $\{d_k, \omega_k\}$ obtained by FDM.
- Eq. 14 using the same set $\{d_k, \omega_k\}$.
- Eq. 13 with $\{d_k, \omega_k\}$ obtained by the Multi-Scale FDM.

No attempt was made to get rid of the noise by throwing away the small entries from the line list. These results demonstrate the following points. (i) Eq. 13 is dangerous to use if there are interfering poles $\omega_k \equiv \nu_k - i\gamma_k$ with both positive and negative "widths" γ_k and big amplitudes d_k. With the slightly wrong formula (Eq. 13 rather than Eq. 14) the negative contributions are not correctly canceled by the positive ones leading to the baseline distortions. Such interference effects are minimized in the Multi-Scale FDM which removes the spurious entries and, in particular, Eq. 13 does not fail.

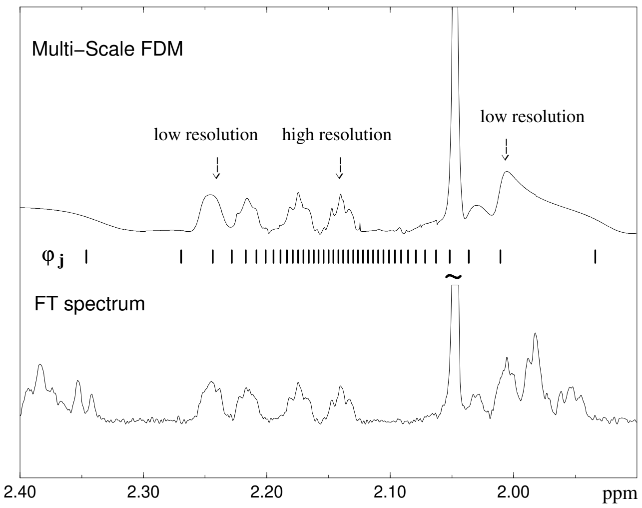

FIG. 4. An example of a multiscale basis set and the spectrum obtained using this basis for the same signal used in Fig. 3. $K_{\text{win}} = 10$ narrow band and $K_c = 20$ coarse basis functions (indicated by an impulse at each φ_j) were used. The coarse functions are distributed non-uniformly according to the displacement from the window: the farther away from the window, the sparser the distribution of the φ_j values.

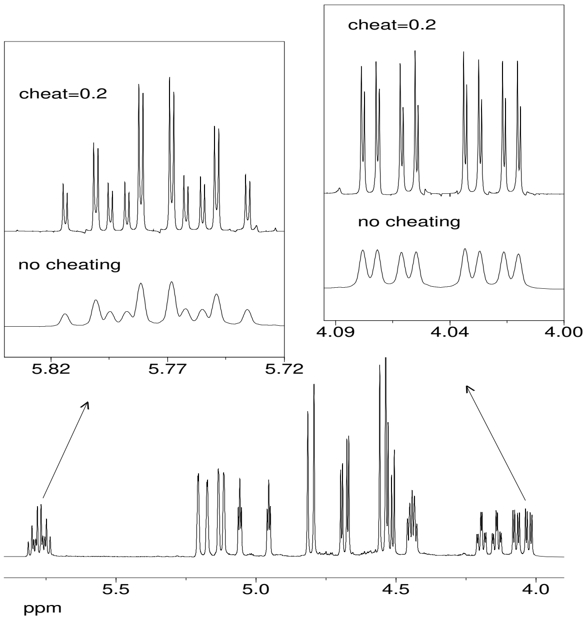

FIG. 5. FDM ersatz spectra of a fluorinated ribose derivative. Both the FDM and FFT (not shown) spectra are absolutely converged with respect to the size, N, of the signal in the sense that further increase of N does not improve the resolution. However, when Eq. 82 is used with cheat $= 0.2$ the doublet structure, hidden in the conventional spectral representation because of the overlapping Lorentzians, is uncovered for all the peaks in the two multiplets shown in the upper traces.

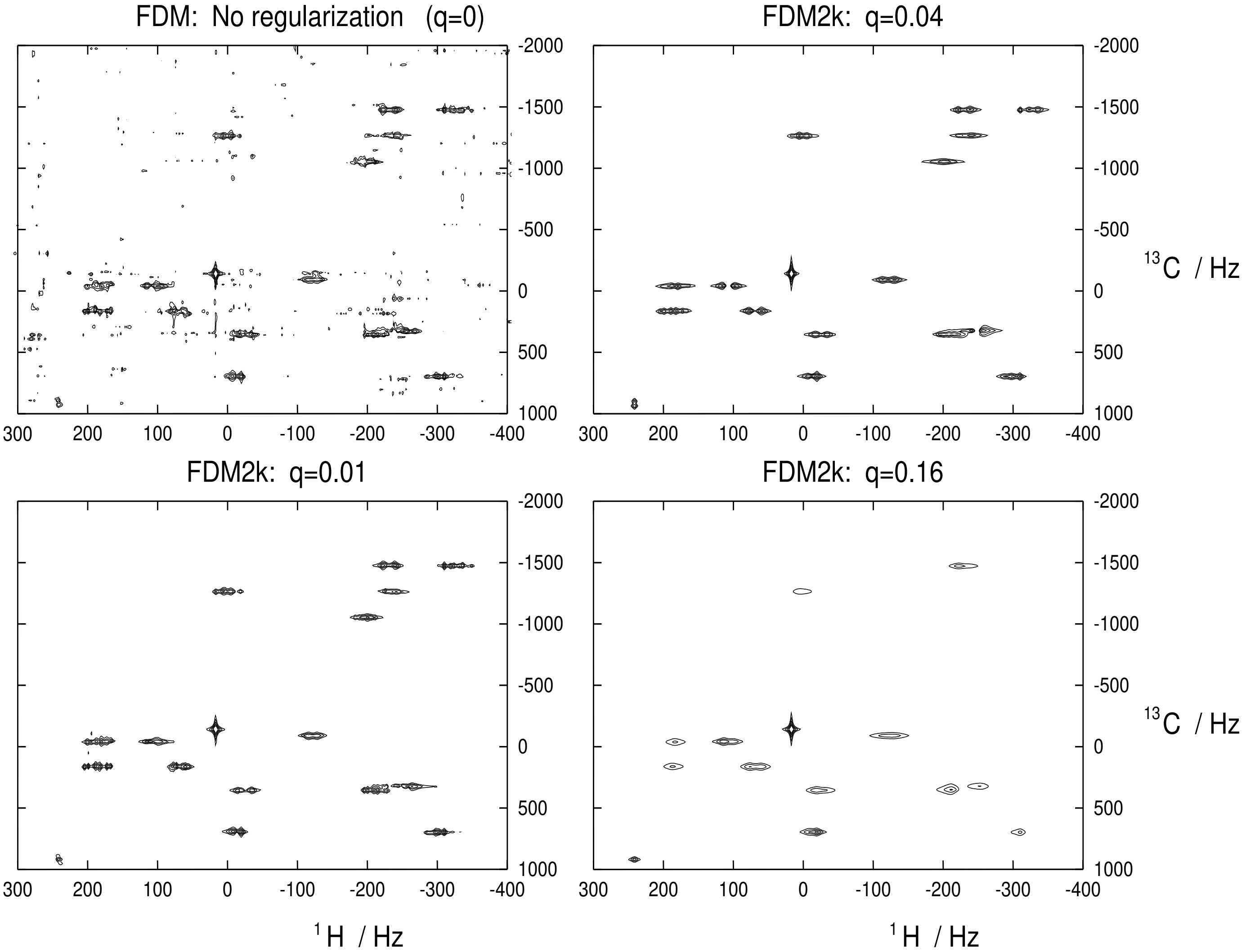

FIG. 6. A non-regularized ($q = 0$) and regularized ($q > 0$) spectra using FDM2k (see Eq. 129) applied to a purely phase modulated 2D signal, generated by an HSQC pulse sequence applied to progesterone (see refs. [6, 13] for more detail). The data set processed consisted of $N_1 \times N_2 = 600 \times 64$ in the proton and the carbon-13 dimensions, respectively. Only a small crowded region of the spectrum is shown, the spectral widths being $SW_1 = 2000$ Hz and $SW_2 = 8625$ Hz. The spectra were generated by combining the results of 8 small overlapping windows, each described by $K_{\rm win} = K_{1\rm win} \times K_{2\rm win} = 24 \times 12 = 288$ Fourier basis functions.

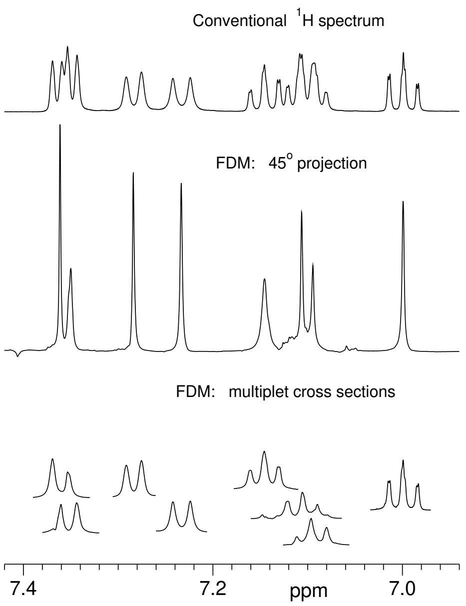

FIG. 7. An example of direct calculation of a 1D 45^o projection and multiplet cross sections by FDM. The spectra were obtained using a purely phase modulated 2D-J signal of ditryptophan tripeptide [9] with just $N_2 = 4$ points along the J-dimension. $N_{\rm FDM} = 20$ calculations with different number of points along the running time dimension in the range $N_1 = 11000 - 12000$ were added together to obtain artifact free spectra (see Section 10.1). Only a small part of the spectrum is shown, while the two spectral widths are $SW_1 = 80$ Hz and $SW_2 = 8$ kHz.

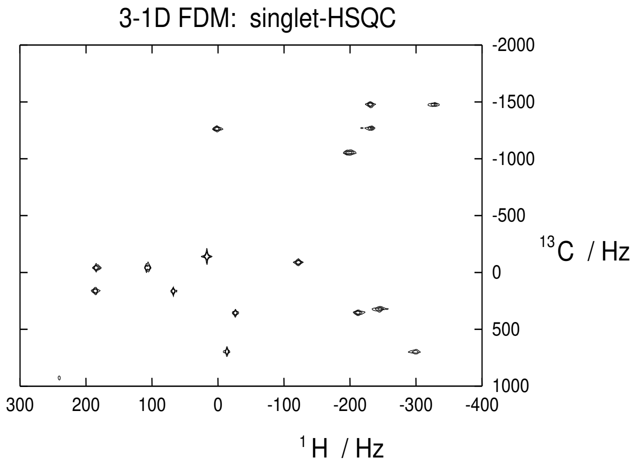

FIG. 8. The *singlet*-HSQC spectrum of progesterone obtained using the pulse sequence of ref. [13]. All the proton multiplets are collapsed into singlets! The 3D purely phase modulated signal consisted of $N_1 \times N_2 \times N_3 = 600 \times 64 \times 2$ points in the proton, carbon-13, and proton J dimensions, respectively. The same, as in Fig. 6, small and crowded spectral region is shown and the same FDM parameters for the windows and basis sizes were used. Here, the regularization was carried out by adding together $N_{\rm FDM} = 50$ calculations with different number of points along the running time dimension in the range $N_1 = 500 - 600$ to obtain an artifact free spectrum (see Section 10.1).